Sensory-neuron subtype-specific transcriptional programs controlling dendrite morphogenesis: genome-wide analysis of Abrupt and Knot/Collier

Yukako Hattori[1], Tadao Usui[1], Daisuke Satoh[1], Sanefumi Moriyama,[2, 3] Kohei Shimono[1], Takehiko Itoh[4], Katsuhiko Shirahige[5], Tadashi Uemura[1, 6]

[1] Graduate School of Biostudies, Kyoto University, Kyoto 606-8501, Japan

[2] Kobayashi-Maskawa Institute, Nagoya University, Aichi 464-8602, Japan

[3] Graduate School of Mathematics, Nagoya University, Aichi 464-8602, Japan

[4] Graduate School of Bioscience and Biotechnology, Tokyo Institute of Technology, Kanagawa 226-8501, Japan

[5] Institute of Molecular and Cellular Biosciences, University of Tokyo, Tokyo 113-0032, Japan

[6] To whom correspondence should be addressed

Running headline: Transcriptional programs shaping dendritic arbors

Author for correspondence: Tadashi Uemura

Graduate School of Biostudies, Kyoto University, Kyoto 606-8501, Japan

(Phone) +81-75-753-9238

(Fax) +81-75-753-4265

(E-mail) tauemura@lif.kyoto-u.ac.jp

Highlights:

- In vivo binding sites (BSs) and expression profiling identified 429 target genes
- The BSs were enriched in tissue specific enhancers and Polycomb chromatin
- Targets with a broad range of molecular functions execute dendritic arbor formation
- One common target gene *Ten-m* controls dendritic branch sprouting or extension

Keywords: sensory neuron; dendrite; transcription factor; neuronal subtype; differentiation; Abrupt; Knot/Collier; DamID; genome informatics; microarray; tiling array; chromatin signatures; modENCODE; postmitotic neuron; cell adhesion molecule; Teneurin; *Drosophila*

eTOC:

Precise differentiation of neuronal subtypes ensures functional nervous systems. We performed genome-wide analyses of postmitotic-subtype selectors of *Drosophila* sensory neurons, Abrupt and Knot. We identified target genes and showed how differentiating neurons employ distinct and shared repertoires of gene

expression to produce subtype-selective morphological traits.

SUMMARY

The transcription factors Abrupt (Ab) and Knot (Kn) act as selectors of distinct dendritic arbor morphologies in two classes of *Drosophila* sensory neurons, termed class I and class IV, respectively. We performed binding-site mapping and transcriptional profiling of isolated these neurons. Their profiles were similarly enriched in cell-type-specific enhancers of genes implicated in neural development. We identified a total of 429 target genes, of which 56 were common to Ab and Kn; these targets included genes necessary to shape dendritic arbors in either or both of the two sensory subtypes. Furthermore, a common target gene, encoding the cell adhesion molecule Ten-m, was expressed more strongly in class I than IV, and this differential was critical to the class-selective directional control of dendritic branch sprouting or extension. Our analyses illustrate how differentiating neurons employ distinct and shared repertoires of gene expression to produce class-selective morphological traits.

INTRODUCTION

In early neural development, cell diversification occurs on a large scale, with extraordinary precision, to generate an enormous number of neuronal subtypes. The specified neuronal types can be distinguished from one another on the basis of a number of criteria of terminal differentiation, ranging from anatomies to electrophysiological properties (Sugino et al., 2006). The cell-intrinsic mechanism yielding these variations operates mostly through transcriptional networks (Bertrand et al., 2002; Hobert et al., 2010; Southall and Brand, 2009), and several key transcriptional factors (TFs) operant in postmitotic cells have been identified (Dalla Torre di Sanguinetto et al., 2008; Fishell and Hanashima, 2008; Vrieseling and Arber, 2006). However there have been few systematic searches for binding profiles of these TFs in the genome, or inventories of their target genes. Consequently, when we focused on TFs that direct distinct traits of multiple subtypes within the same category of neurons, little was known about how divergent the corresponding binding sites and target genes would be.

One of the signature neuronal hallmarks exploited for this study is the diverse morphology of the dendritic arbor, which supports differential processing of synaptic or sensory inputs, thereby realizing functional variations (Hausser and Mel, 2003; Jan and Jan, 2003; London and Hausser, 2005). The underlying transcriptional programs can be revealed with appropriate model systems, such as the stereotyped organization of identified dendritic arborization (da) neurons in

Drosophila, which have contributed much to the physiological functions of nociception and proprioception (Corty et al., 2009; Grueber et al., 2002; Im and Galko, 2012; Jan and Jan, 2010; Landgraf and Evers, 2005). At the mature larval stage, da neurons in the abdominal hemisegment are classified into 4 categories, classes I-IV, in order of increasing territory size and/or branching complexity (Grueber et al., 2002) (Figure 1A-1D). Class I neurons are characterized by formation of simple comb-like small dendritic arbors (Figure 1A), whereas class IV neurons develop far more complicated and expansive ones (Figure 1B).

A group of TFs play pivotal roles in this class specification in postmitotic cells. The founding member is a homeodomain protein, Cut (Ct), which is differentially expressed among the three classes II-IV and controls class-specific arbor shapes (Grueber et al., 2003). In addition to this multi-level selector, a BTB-zinc finger protein Abrupt (Ab) and a member of the Early B-Cell Factor/Olfactory 1 family, Knot (Kn; also designated as Collier), are selectively expressed in class I and IV, respectively, and each endows the class-I or IV-specific dendritic pattern (Crozatier and Vincent, 2008; Hattori et al., 2007; Jinushi-Nakao et al., 2007; Li et al., 2004; Sugimura et al., 2004) (Figure 1C and 1D). Several target genes of these TFs are known or suggested by candidate approaches (Crozatier and Vincent, 2008; Hattori et al., 2007; Jinushi-Nakao et al., 2007); however, genome-wide views have hitherto not been presented. Here we focused on transcriptional programs that are directed by the class I selector Ab and the class IV selector Kn. We searched for target genes of Ab and/or Kn on a whole genome

scale to better understand how each TF regulates class-selective differentiation, and highlighted a subset of the target genes that are required for shaping the dendritic arbors of both or either of class-I or IV; we then focused on a particular target gene, and how it contributes to producing the class-selective morphological traits.

RESULTS

In vivo binding sites (BSs) and expression profiling identified 429 Ab and/or Kn target genes, out of which 56 were common

To identify target genes regulated by Abrupt (Ab) and Knot (Kn), we started profiling in vivo binding sites (BSs) by the DamID method (Choksi et al., 2006; van Steensel et al., 2001; van Steensel and Henikoff, 2000). On the basis of our objective standards, we defined BSs of each TF, as well as Ab- or Kn-“bound” genes (Figure 2A, S2, and Table S1). 48% of the bound genes of one TF were overlapped by the other (Figure 2B). The common bound genes are designated as the Ab/Kn-bound genes hereafter.

The above BS data did not yield information about whether they are target genes in da neurons or not, since Ab and Kn are also expressed in cell types other than da neurons (Dubois et al., 2007; Hu et al., 1995). To complement our DamID analysis, we isolated da neurons from larvae and obtained genome-wide expression

profiles under the conditions where ectopic expression of *ab* or *kn* in all classes of da neurons severely affected morphologies of dendritic arbors (Figure 1E-1G'), presumably due to altered levels of transcription of target genes of each TF. For simplicity, we designated this expression style as misexpression or ME throughout this study. We identified 1508 genes that were up- or down-regulated by *ab* ME and 451 by *kn* ME (Figure 2C, 2D). These genes were designated as *ab*- or *kn*-"dependent" genes (Figure 2F and 2G, and Table S1D and S1E).

Cross-referencing the *ab* ME data set with the set of the Ab-bound genes showed that 196 up-regulated and 190 down-regulated genes were identified as Ab-bound genes. Thus, we designated these 386 genes as Ab "target" genes, or simply "targets" hereinafter (Figure 2C, 2E, and Table S1F), and strictly distinguished them from the bound genes that were defined on the basis of the DamID data alone. Likewise, 99 *kn*-dependent genes (59 up and 40 down) were designated as Kn target genes (Figure 2D, 2E, and Table S1G). We confirmed the increase or the decrease in the expression levels of a subset of target genes by immunohistochemistry and/or qPCR (Table S2; see also Figure S1). For example, the expression of *lola*, one of the up-regulated targets of Ab and Kn, is increased in *ab* ME or *kn* ME larvae, and decreased in *ab* or *kn* mutant embryos (Figure S1). The fact that the number of Ab targets identified is four-times more than that of Kn targets might reflect the longer duration of Ab expression (from embryos till mature larvae) than that of Kn expression, which is no longer detected in the larvae (Shimono et al., 2009) (Figure 1D). The total number of Ab and/or Kn targets was 429, of which 330

(85%) were specific to Ab (Figure 2E). The number of up-regulated or down-regulated genes suggests that Ab and Kn act as both transcriptional activators and repressors.

One naive expectation had been that at least a subset of the 56 common target genes would be regulated by Ab and Kn in opposite ways. Unexpectedly however, there were no such targets; each of the 56 common target genes was either up-regulated by both Ab and Kn, or down-regulated by both Ab and Kn. We thought it possible that some common targets are regulated by the two TFs in quantitatively differential fashions, and such candidates are lined up in our microarray analysis under the *ab* ME or *kn* ME conditions (Table S1H). In fact, we confirmed such differential control of gene expression when we examined individual target genes, such as *lola* and *Ten-m* (discussed later). Out of the complete lists of the *ab* or *kn*-dependent and the bound genes (Table S1C), those implicated in neuronal differentiation or neuronal functions and miRNA genes are selected and enumerated in Table S3.

The BSs of Ab and/or Kn target genes were enriched in genomic regions that are classified into tissue specific enhancers and Polycomb chromatin

To compare BSs of Ab and/or Kn with those of other TFs, we clustered BSs for a total of 35 TFs and found a strong correlation between the Ab BSs and Kn BSs (Figure 3A). This result strengthened the possibility that the Ab/Kn-bound genes are transcriptionally regulated in (a) similar developmental context(s). This possibility

appears to be consistent with our survey of Gene Ontology (GO) annotations of the Ab-bound genes and the Kn-bound ones, which showed a highly significant overrepresentation of the terms such as “neuron differentiation” in both gene groups (Figure 3B and 3C). Our clustering also showed that both the Ab BSs and the Kn BSs were highly correlated with the BSs of a transcriptional co-repressor Gro that is shown to control class I dendrite morphogenesis (Parrish et al., 2006) (Figure 3A).

We then inspected the BSs of Ab or Kn by taking advantage of integrative data sets of histone modifications and chromatin components (Figure S3A). Chromatin features of the *Drosophila* genome have been classified into five “chromatin types” defined by DamID analysis (Filion et al., 2010). We confirmed that the combinatorial patterns of enrichments or paucities of the markers (such as those shown in Figure S3A) are basically conserved among the cell lines, embryos that we used for DamID, and third-instar larvae from which we isolated da neurons for the expression profiling (Figure S3B and S3C; see legend), although it would be ideal to obtain neuronal class-specific data sets and respective chromatin landscapes for each class of da neurons. For both Ab and Kn, the most prominent selectivity was manifested by the large fractions of the target BSs, especially the BSs of up-regulated targets, in the RED chromatin type that is transcriptionally active in a tissue-specific fashion (Filion et al., 2010) (Figure 3D and 3E). Another less conspicuous but significant enrichment was seen in genomic regions that are marked by Polycomb group (PcG) proteins or “Polycomb chromatin” (BLUE). It should be noted that BLUE chromatin may not invariably mean transcriptionally

silenced regions; one proposal is that a subregion of Polycomb chromatin is in a "balanced state," where Polycomb group proteins and active markers coexist (Schwartz et al., 2010). BSs of the transcription factor Prospero (Pros), which acts as a binary switch between self-renewal and differentiation in neural stem cells (Choksi et al., 2006), were also prevalent in RED (see Pros BSs in Figure 3D and 3E). Essentially the same results were obtained on the basis of another classification of chromatin features ("chromatin states"; (Kharchenko et al., 2010); Figure S3B, S3D and S3E; see also Figure S1I).

Targets with a broad range of molecular functions execute dendritic arbor formation in a class-selective or common fashion

To examine roles of the target genes in dendrite morphogenesis, we selected 103

target genes out of the 429 on the basis of GO annotations and carried out their knockdown and/or overexpression in class I and IV neurons (see details in Supplemental Experimental Procedures). Listed in Table S4 are 24 target genes whose knockdown phenotypes were validated with two distinct dsRNA sequences, for which expression and/or overexpression caused malformation of dendritic arbors. As for target genes whose null or strong alleles have been reported, we examined phenotypes of mutant neurons and obtained results essentially consistent with those obtained by knockdown analysis (Figure S4A-S4J, S4O-S4Q). Many of these targets are conserved across species and have eluded previous knockdown or mutant screenings of dendrite morphogenesis (Gao et al., 1999; Parrish et al., 2006; Satoh et al., 2008; Ye et al., 2007; Zheng et al., 2008).

We expected that Ab targets and Kn targets would be transcriptionally up- or down-regulated by Ab in class I da neurons and by Kn in class IV, respectively, and such regulations would be required for sculpting dendrite arbors in each class-selective fashion. Indeed, *spinster* (*spin)*, encoding a protein implicated in endosome-to-lysosome transport (Dermaut et al., 2005; Sweeney and Davis, 2002), is one of the up-regulated targets of Ab*,* and its knockdown deformed the comb-like shape of class I arbors (Figure 4A and 4B). Secondary branches, which are supposed to grow along the anterior-posterior axis (A-P axis) in a parallel manner, were misoriented to each other; consequently, the arbor size increased compared to that of the control, although the terminal number did not (Figure 4K-4L). Likewise, one of the Kn targets, *CG14642*, which is predicted to encode a protein with a

serine-type endopeptidase activity, was required specifically for spatial control of branching within the class IV arbor (Figure 4F and 4G). This was evidenced by the fact that *CG14642* knockdown caused a significant shift of branching activity to the proximal area in the arbor (Figure 4O).

In contrast to the Ab or Kn selective targets, the common targets were expected to play important roles in both class I and IV neurons. Consistent with this prediction, knockdown of four up-regulated targets significantly deformed both class I and IV arbors (Figure 4C-4D, 4H-4I, Table S4, and Figure S4A-S4D), as shown by the decrease either in the terminal number (Figure 4K, 4M) or in the length per branch (Figure 4N), or by misdirections of branch extension (Figure 6-8; explained later). These targets are *dOrai*/*Olf186-F*, *lola*, *CG31431*, and *Ten-m*, which encode a Ca2+ release-activated Ca2+ channel (Agrawal et al., 2010; Venkiteswaran and Hasan, 2009), a transcription regulator that controls neural development (Giniger et al., 1994; Spletter et al., 2007), a putative fibroblast growth factor-activated receptor, and a type-II transmembrane protein Ten-m (that is further characterized below), respectively. To examine whether the molecular network that includes dOrai controls dendritic arborization or not, we knocked down the gene encoding Stromal interaction molecule (dSTIM) that is localized on the ER and binds to dOrai, or *iptr* encoding the IP_3 receptor. The knockdown of *dSTIM* or *iptr* also significantly reduced the number of class I and class IV branches (Figure S4K-S4N, S4R, and S4S), supporting a critical contribution of the intracellular Ca2+ homeostasis regulation pathway in both classes. On the other hand, knockdown of some of the

common targets caused severe phenotypes in one of the two classes, and these include *Imp*, *Pak3*, or *tai* of the up-regulated group. For example, Knockdown of *Insulin growth factor II mRNA binding protein* (*Imp*), implicated in RNA localization and stabilization (Adolph et al., 2009; Boylan et al., 2008; Yisraeli, 2005), dramatically reduced the length of class IV arbors, but its effect on class I was not detected, at least with regard to the number of branch termini (Figure 4E, 4J, 4K, 4N, S4E-S4H, S4O-S4Q).

Our overexpression experiments raise the possibility that quantitative control of expression of some of the target genes is critical for proper arbor development of class IV. For example, in contrast to the severe simplification of the arbor by the *Imp* knockdown as described above (Figure 4J), its overexpression increased the branch number (Figure 5A, 5C, and 5I). As for *lola*, both knockdown and overexpression resulted in arbor simplification (Figure 4I and 5D). It is thus possible that the *Imp* and *lola* levels must be adequately controlled to determine the arbor complexity. Another instance was given by *spin* overexpression, which simplified class IV arbors (Figure 5B). These phenotypes are consistent with a hypothesis that *spin* expression should be repressed below a certain level for normal class IV development.

We further assessed the biological relevance of the targets in the context of Kn misexpression-induced transformation of dendritic arbor shapes. Misexpression of Kn in class I neurons increases the number of higher-order branches and deforms the comb shape, which we designate as a class IV-like transformation (Hattori et al.,

2007) (Figure 5E and 5F). We assumed that up-regulation of the Kn target genes most likely contributed to this class IV-like transformation. To verify this hypothesis, we misexpressed Kn in class I neurons with concurrent knockdown of individual Kn target genes. Out of the six up-regulated targets which we showed were required for class IV arbor formation, knockdowns of five significantly suppressed the class IV-like transformation phenotype of class I neuron ddaE (Figure 5G, 5H and 5J; Table S4). These results of our integrated approaches identified a group of target genes that were bound by either key TF, were transcriptionally regulated, and contributed to morphological diversification of the two classes of the da neurons.

Knocking down a common target gene, *Ten-m*, in class I or IV altered directional features of branch sprouting or extension

To obtain mechanistic insights into the morphological diversification of dendritic arbors achieved by Ab and Kn target genes, we studied one of the common target genes, which encodes a homophilic cell adhesion molecule of the teneurin family, Ten-m, in further depth. Ten-m is necessary for pathfinding decisions in motor axon navigation (Zheng et al., 2011) and instructs synapse organization in the olfactory circuit and at neuromuscular junctions (Hong et al., 2012; Mosca et al., 2012). We first showed that *Ten-m* RNAi worked efficiently in class I and IV neurons (Figure S5H-S5I') and examined knockdown phenotypes (Figure 6-7).

We focused on the morphological features of class I ddaE, whose secondary branches sprout from the dorsally-oriented primary ones, with a

significant posterior preference (Figure 6A). Those secondary branches extend along the anterior (A)-posterior (P) axis. The knockdown abrogated the directional preference of the branch sprouting, making comparable numbers of secondary branches sprout in both A and P directions (Figure 6B and 6M). We also examined another class I vpda (Figure S5A-S5C; see legend).

To characterize phenotypes of class IV ddaC, we performed quantitative analyses using several parameters and found a significant alteration in neither the total dendrite length, the number of branch termini, nor spatial disposition of branches within the dendritic arbor (data not shown). Instead, we found that the knockdown showed a significantly biased directional distribution of terminal branches (Figure 7A, 7B, 7G-7H', 7O, and 7P). Compared to the control ddaC, branches under the knockdown conditions extended in a less radial manner.

Ten-m was more highly expressed in class I than IV, and in overlying epidermis in a non-uniform fashion

Considering that various types of neurons employ Tenurins to pair with target cells expressing the same Tenurin subclass (Hong et al., 2012; Leamey et al., 2007), we speculated that dendritic branches of the da neurons might interact with adjacent cells by way of homophilic interactions of Ten-m. To explore this possibility, we primarily monitored *Ten-m* expression by detecting the *Ten-m* enhancer-dependent expression of a reporter in the respective *GAL4* enhancer trap line (Hong et al., 2012) and found that Ten-m was expressed both in class I and class IV neurons and

also in non-neuronal tissues such as epidermis, a subset of muscles (Mosca et al., 2012), and hemocytes (Figure 6E-6F, 6H, 6H', and S5D-5E). The expression patterns were intriguingly differential in two respects: (1) Ten-m was expressed much more strongly in class I than class IV (Figure 6E, 6E', 6H, and 6H'), which is consistent with higher activation by *ab* ME than *kn* ME (Table S1H). We also showed that this expression in class I was reduced in the *ab* mutant (Figure 6I and 6J), which validated our identification of *Ten-m as* one of the Ab target genes. In addition to the *Ten-m* enhancer-dependent reporter expression, we found that endogenous Ten-m signals were much stronger in class I than class IV (Figure S5F-S5G'). (2) The expression in the epidermis, which makes direct contacts with dendrites (Han et al., 2012; Kim et al., 2012; Parrish et al., 2009), was non-uniform. It was higher in a stripe about three epidermal cells wide, encompassing neuronal cell bodies and proximal dendrites, than in the more distal zone (Figure 6E-6G). *Ten-m* expression has already been initiated in both the neurons and the neighboring epidermal cells in the first instar larva (Figure S5E). These results allowed us to posit that Ten-m may work both in the neuron and adjacent tissues to prompt dendrite patterning, and that the imbalance of Ten-m in the epidermis provides the directional cue for the branch sprouting of class I ddaE from the higher to lower Ten-m level.

Knocking down or overexpression of *Ten-m* in adjacent tissues also abrogated directional features of branches

Next, we examined phenotypes of class I ddaE and class IV ddaC, when *Ten-m* was knocked down or overexpressed in adjacent tissues. To analyze knockdown phenotypes of ddaE, the drivers employed were *Ten-m-GAL4* for knockdown in all *Ten-m*-expressing cell types, and *arm-GAL4* for knockdown in adjacent tissues such as epidermis and muscles (Parrish et al., 2009). All knockdowns tested abrogated the directional preference of the branch sprouting (Figure 6C-6D' and 6M). To verify the hypothesis that the imbalance of Ten-m in the epidermis provides the directional cue for the branch sprouting, we overexpressed *Ten-m* in the *hh* domain within epidermis (Figure 6K-6L'), where *Ten-m* expression during development is normally much lower than in the proximal dendrite zone (Figure 6F). In control larvae, secondary dendrites grew in the *hh* domain (Figure 6K and 6K'); in striking contrast, branches were hardly seen in the *Ten-m* overexpressing domains (Figure 6L, 6L', and 6N). Moreover, the normal directional bias of sprouting of ddaE secondary branches was significantly impaired (Figure 6M). These results suggested that the dendritic branches did not ascend the presumptive counter slope of Ten-m in the epidermis. These results of the knocking down or overexpression experiments are consistent with our hypothesis.

To address whether *Ten-m* in adjacent tissues contributes to dendrite morphogenesis of class IV ddaC or not, we knocked down *Ten-m* in all *Ten-m*-expressing cell types (Figure 7C, 7D, 7I-7J', 7Q, and 7R). In addition, we knocked down *Ten-m* selectively in the *hh* domain in the epidermis (see green zones in Figure 7E and 7F) that belongs to the Ten-m-low distal zone (Figure 7E, 7F,

7K-7L', 7S and 7T). Compared to the control ddaC, extension of terminal branches under either knockdown condition was significantly biased along the A-P axis (Figure 7S-7T), as it was when *Ten-m* was knocked down in the neuron (Figure 7O and 7P). Importantly, the directional distribution of terminal branches was not altered on the side opposite to the *hh* domain (magenta zones in Figure 7E and 7F, 7M-7N' and Figure 7U and 7V), strongly suggesting that the *Ten-m*-mediated dendrite-epidermis interaction locally contributed to orienting terminal branches in the wild type. These results lead us to speculate that in normal development the ddaC dendrites, once they enter the Ten-m-low zone, are prompted to arborize and direct their termini essentially in all directions, which most likely allows efficient coverage of the body surface with branches (Grueber et al., 2002).

Ten-m overexpression in class IV endowed a directional preference of branch extension, which is reminiscent of the normal class I arbor

The above results show that *Ten-m* was necessary for normal arbor formation of both classes. Then how does this common target gene produce the class-selective morphological traits? We were intrigued by the finding that class IV ddaC expressed *Ten-m*, but at a much lower level than class I ddaE (Figure 6H, 6H', S5F, and S5F'). So we addressed whether overexpression of *Ten-m* in ddaC affected its dendrite morphogenesis or not (Figure 8). The control ddaC neurons directed their branch termini to A and P directions nearly equally (Figure 8A, 8A', and 8E); in contrast, branch growth of *Ten-m*-overexpressing ddaC showed a posterior preference

(Figure 8B, 8B’, and 8E), which is reminiscent of a directional feature of the ddaE secondary branches (Figure 8C, 8C’, and 8E). This phenotype of the *Ten-m* overexpressing-ddaC was not associated with a net decrease of the branch number (Figure 8F), excluding the possibility that the ddaE-like posterior preference was a consequence of overall arbor simplification. These results could be interpreted to mean that the elevated level of Ten-m in ddaC branches makes them respond to the higher-to-lower level of epidermal Ten-m towards the posterior border in each hemisegement, as class I ddaE does.

All of our results strongly suggest the possibility that the Ten-m-mediated interaction between dendritic branches and the epidermis produces the distinct directional outputs of branch growth in neuronal subclass-specific fashions (Figure 8G). In class I ddaE, the Ten-m-high dendrites responded to the epidermal high-low Ten-m imbalance, realizing the predominantly posterior-oriented comb-like pattern of class I ddaE; in class IV ddaC, the low-level expression in the neurons and the epidermis ensures the relatively radial pattern of terminal branches. Thus our data of Ten-m provides mechanistic insights into how the differential expression of Ten-m contributes to producing the class-selective morphological traits.

DISCUSSION

The transcriptional programs of our focus were predicted to be more specialized for

controlling neuronal terminal differentiation at postmitotic stages, compared to those in which proneural genes, such as Asense and its vertebrate homolog Ascl1 (Mash1), regulate cell proliferation or cell cycle arrest and also promote differentiation (Castro et al., 2011; Southall and Brand, 2009). Indeed, predicted molecular functions of Ab and Kn target-coded proteins are diverse, ranging from transcriptional control to cell adhesion, membrane trafficking, Ca2+ entry, and cytoskeleton regulation. Then how do these targets contribute to shaping dendrite arbors in the class-selective fashion?

Our genome-wide study strongly supports the notion that the class selectors do indeed control transcription of target genes selectively. On the other hand, both TFs have chromatin features of the BSs in common and show the same directional (up or down) regulation of every common target. To explain these findings, we were intrigued by the possibility that some common targets might be regulated by the two TFs in quantitatively differential fashions. As a precedent, Cut (Ct) is differentially expressed among the three classes (class II-IV), which controls formation of the different branching patterns and the growth of dendritic arbors of individual classes (Grueber et al., 2003). In this study, compelling data for the above hypothesis was obtained by our analyses of a common target, *Ten-m*. Its high-level expression in class I ddaE endowed its branches with the capability to respond to the decreasing level of Ten-m in the epidermis, thus setting the directional preference of branch sprouting (left, in Figure 8G). In contrast, a much lower expression in class IV ddaC ensured the directing of terminal branches rather

radially in the distal area of each arbor, where the overlying epidermal *Ten-m* expression is low (right, in Figure 8G). These level-dependent roles of Ten-m could be related, or analogous to a role of mouse Ten-m3 in navigating Ten-m3-high retinal projections to the high target region (Leamey et al., 2007; Young and Leamey, 2009) and those of Tenurins in instructing synaptic partner matching in the *Drosophila* olfactory map (Hong et al., 2012). It awaits further study to reveal how the differential levels of Ten-m produce the class-selective directional properties of branch patterning, possibly by way of organization of cytoskeletons and membranes (Mosca et al., 2012).

Our other experimental results are also consistent with the critical role of the quantitative control of target gene expression. First, the amount of Lola, one common target-gene product, was higher in class I ddaE than class IV ddaC in a wild type background (Figure S1). Second, results of knockdown and overexpression of *Imp* and *lola* indicate that their expression levels must be strictly controlled to determine the arbor complexity. Third, we had superficially puzzling findings about down-regulated targets (those with decreased expression upon *ab* or *kn* ME). In the narrowed-down list of Ab target genes (Table S4), 10 targets were down-regulated by *ab* ME, and their knockdown in class I (which expresses Ab endogenously) yielded obvious abnormal phenotypes. Ab may keep the transcription of the down-regulated targets weakly active, and does not totally shut down the expression; moreover, this low-level expression may be required for normal class I development. To test these hypotheses, what would be required is

class-selective quantitative expression profiling, ideally at multiple developmental stages, including the onset of primary dendrite formation and a subsequent branch growing phase.

85% or more of the bound genes were not identified as exclusively Ab and/or Kn-dependent genes; and it could be that Ab and Kn may be able to control transcription of some of those in conjunction with other TFs. Candidate bound genes of this group include Kn-bound genes *Ubx* and *abd-A*, that are silenced in class IV by PcG proteins (Parrish et al., 2007), which showed a similar binding profile with Kn, while an unknown transcriptional co-activator may drive expression of *turtle*, which is an Ab/Kn-bound gene necessary in class I and IV (Long et al., 2009). Furthermore, with respect to physiological functions of proprioceptive class I and multi-modal nociceptive class IV, it should be mentioned that *Gr28b* encoding a bright blue light sensor was a Kn-bound gene (Table S3A). Additional profiling data sets, such as that in the co-presence of Kn and Ct, will deepen our understanding of the intricate transcription codes, with the ultimate goal of identifying the molecular links between the codes and the diverse architectures of dendritic arbors and neuronal functions.

EXPERIMENTAL PROCEDURES

All details including exact genotypes of individual animals used in figures are described in SUPPLEMENTAL INFORMATION.

DamID

We expressed Ab or Kn, which had been fused with the Escherichia coli DNA adenine methyltransferase (Dam), at a very low, i.e. leaky, level in embryos in order to methylate GATC sequences adjacent to the BSs of the respective TFs. We amplified methylated genomic fragments and hybridized them to tiling arrays. Data of four independent replicates of the arrays were processed to determine the representative BS profile (Figure S2).

Databases

Throughout this study, genomic sequence coordinates of *Drosophila* melanogaster followed FlyBase genome Release 5.0 (McQuilton et al., 2012); and the reference gene list employed was FlyBase r5.35 containing a total of 15,191 genes. *Drosophila* modENCODE data (http://www.modencode.org/) and the genome-wide data of the chromatin signatures have been described (Filion et al., 2010; Kharchenko et al., 2010; Negre et al., 2011).

Expression profiling of isolated da neurons

To complement our DamID analysis, we isolated da neurons from larvae using magnetic beads, prepared RNA basically as described (Iyer et al., 2009) with modifications, and obtained genome-wide expression profiles.

Functional Annotation Classification of Genes using Gene Ontology

For this clustering, an overrepresentation analysis for Gene Ontology (GO) entries was carried out. To this end, a Fisher's test was employed as implemented in the DAVID Bioinformatics Resource (Dennis et al., 2003). As a reference gene list, all genes from FlyBase r5.35 entries were used. Results are presented by either P-values that were adjusted using Benjamini-Hochberg's multiple testing correction method (Figure 3B and 3C) or enrichment score (Huang da et al., 2009) (Figure 2F and 2G).

Public database access of microarray data

The raw and processed data for the DamID- binding experiments and the expression profiling experiments described here are available on the GEO public database (http://www.ncbi.nlm.nih.gov/projects/geo/). The accession numbers are as follows: DamID data sets—GSE38659. Expression profiling—GSE38660.

Imaging dendritic trees, immunohistochemistry, in situ hybridization, quantification, and statistical tests

Protocols of single cell labeling (MARCM), imaging, quantitative analysis of the

images, immunohistochemistry, and in situ hybridization were essentially as described (Hattori et al., 2007; Matsubara et al.; Yamamoto et al., 2006). Images were acquired from wandering 3rd instar wandering larvae unless described otherwise. Antibodies employed for immunohistochemistry include anti-GFP (B2 of Santa Cruz), anti-Lola (Giniger et al., 1994), anti-Ten-m (Baumgartner et al., 1994; Levine et al., 1994), and Alexa Fluor 488- or Cy3-conjugated anti-HRP (Jackson ImmunoResearch). We followed (Grueber et al., 2003) for quantification of Lola signals (Figure S1D-S1H). For quantification of mCD8:GFP signals in epidermis (Figure 6E'), we drew an epidermal region of interest (ROI) 10 μm in diameter, which did not include dendrites, and calculated the intensity per pixel. From each dorsal cluster, three ROIs were chosen, and each data point in Figure 6G represents an average pixel intensity of each ROI.

The statistical tests employed are one-way ANOVA and HSD *post-hoc* test or Wilcoxon-Mann-Whitney test, and KaleidaGraph (Synergy Software) was used for the calculations. Circular statistics and rose plots were generated in Oriana 4 (Kovach Computing Service) and PAST (Hammer, 2001). The frequency of observations in rose plots is represented by the area of each wedge.

ACKNOWLEDGEMENTS

The reagents, genomic datasets, and/or facilities were provided by the *Drosophila* Genetic Resource Center at Kyoto Institute of Technology, the NIG stock center, the Bloomington Stock Center, Vienna *Drosophila* RNAi Center, the TRiP at Harvard

Medical School (NIH/NIGMS R01-GM084947), the Developmental Studies Hybridoma Bank at the University of Iowa, the *Drosophila* Genomics Resource Center (DGRC), FlyBase, modENCODE, Y.N. Jan, C. Han, S. Hayashi, H. Wada, S. Yonehara, Y. Kobayashi, T. Aigaki, D. St Johnston, A. Nose, E. Giniger, G. Davis, N. Harden, S. Adolph, D. Montell. L. Luo, T. Mosca, S. Baumgartner, and R. Wides. We also thank A.H. Brand, T.D. Southall, B. van Steensel, N.M. Luscombe, J.M. Vaquerizas, K. White, M. Ebisuya, T. Yamamoto, Y. Natsume, Y. Shinkai, M. Suyama and E. Nagoshi for advice on informatics or cell isolation and/or related reagents; J. Hejna for polishing the manuscript; and J. Mizukoshi, and M. Futamata for their technical assistance. This work was supported by a grant from the programs Grants-in-Aid for Scientific Research on Innovative Areas “Mesoscopic neurocircuitry” (22115006 to T. Uemura). Y. H. is a recipient of a JSPS Research Fellowship for Young Scientists.

FIGURE LEGENDS

Figure 1. Class I and IV da neurons

(A and B) Dendritic morphologies of class I neuron ddaE (A) and class IV neuron ddaC (B). In this and all subsequent figures, anterior is left and dorsal is up, and images of the dorsal cluster at wandering 3rd instar stage are shown unless described otherwise. (C) Dendrite morphologies of class I-IV da neurons and selective expression of transcription factors (TFs) in each class. (D) Timeline of development of class I and IV da neurons and the temporal expression profiles of Ab and Kn after egg laying (AEL). Adapted from (Yamamoto et al., 2006). Class I neurons almost cease branching at the end of embryogenesis and keep growing preexisting branches in larvae, while class IV neurons continue to elaborate higher-order branches throughout larval stages. Kn was not detected at the 3rd instar wandering larval stage (Shimono et al., 2009). There is no strong evidence for an epistatic relationship between these two TFs (Hattori et al., 2007). (E-G') Effects of Ab or Kn ectopic expression in all classes of da neurons (designated as misexpression or ME for simplicity). Dendritic arbors in the control (E and E'). Downsizing and simplification in the case of *ab* ME (Sugimura et al., 2004) and an increase in complexity with *kn* ME (Hattori et al., 2007). E'-G' are high-power images of boxed areas of E-G. Bars, 100 μm. See also Figure S1.

Figure 2. Genome-wide mapping of Ab and Kn binding sites and identification of the target genes

(A) Examples of DamID data of Ab (green) and Kn (magenta). The 393-494 kb region of chromosome 2L is shown. Bar heights are proportional to averages of standardized log2-transformed ratios of intensities (see details in EXPERIMENTAL PROCEDURES and Figure S2A). Boxes indicate binding sites of each TF (Ab BS and Kn BS). (B) Venn diagram showing the overlap between the bound genes of the TFs. (C-D) Venn diagrams showing the overlaps between the TF-bound genes and TF-dependent genes that were either up-regulated (Up) or down-regulated (Down) by ectopically expressing *ab* (C) or *kn* (D) in all classes of da neurons (designated as misexpression or ME for simplicity in this study). (E) Intersection of the dual genome-wide profiling defined 386 Ab target genes (196+190 in “C”) and 99 Kn target genes (59+40 in “D”), out of which 56 genes are common. Note our designations of Ab-specific targets, Kn-specific targets, and common targets. The Ab targets and the Kn targets comprise just 26% and 22%, respectively, of the TF-dependent genes (386/1508 and 99/451, respectively). Such small or even smaller overlaps in the dual genome-wide profiling (the binding and the expression) have been documented in studies of Foxp3 and Ascl1 in mice (Castro et al., 2011; Zheng et al., 2007). (F-G) GO clusters enriched in Ab- or Kn-dependent genes. The top five gene ontology (GO) clusters enriched in Ab- (F) or Kn-dependent genes (G) in biological process category by enrichment score. See also Figure S2 and Table S1-S3.

Figure 3. Overlaps and ontology of the Ab- or Kn-bound genes, and

enrichment of BSs in tissue-specific enhancers and Polycomb chromatin

(A) Pairwise comparisons of HOT-subtracted BSs of TFs are indicated (HOT: high occupancy target regions or hotspots). Enrichments/depletions are color-coded by fold enrichment. The data sets are from the modENCODE consortium, except for the two of this study (orange boxes) that are located close-by in this clustering (highlighted by black frames; the correlation index of Ab with Kn was 2.2). *gro1* and *gro3* are technical replicates.

(B and C) The top ten gene ontology (GO) clusters enriched in Ab- (B) or Kn-bound genes (C) in biological process categories, ranked by p-value. Each GO cluster was represented by one GO term in the cluster.

(D and E) BSs of Ab, Kn, or Pros were sorted into chromatin types that are defined by the data sets of KC167 cells (Filion et al., 2010). Enrichments/depletions of fractions of individual chromatin types are calculated relative to those in the genome and color-coded by fold enrichment (E). The data of Pros BSs are derived from Table S1 and S3 of (Choksi et al., 2006). Lower limits of the depletion were set to negative values of the maximum enrichment. All: all of the BSs; Up: BSs associated with up-regulated target genes (up-regulated in *ab* ME or *kn* ME, down-regulated in *pros* mutants); and Down: BSs associated with down-regulated target genes (down-regulated in *ab* ME or *kn* ME, up-regulated in *pros* mutants). Most noticeably, RED type chromatin includes 50.0% of the BSs of Ab up-regulated targets (D), and its enrichment is 5.4 fold (red boxes with black frames in “E”). See also Figure S3.

Figure 4. Effects of knockdown of target genes on dendrite morphogenesis of class I or IV

Images of class I neuron ddaE (A-E) and class IV ddaC (F-J). Control (A and F), *spin-RNAi* (B), *dOrai-RNAi* (C and H), *lola-RNAi* (D and I), *Imp-RNAi* (E and J), and *CG14642-RNAi* (G). (K-O) Quantitative analyses. The terminal number (K) and the size (L) of the ddaE arbor. The terminal number (M), cumulative branch length divided by the terminal number (N) of the dorsal side, and the terminal number of the proximal region (O; the boxed 200μm x 200μm regions in F and G) of the ddaC arbor. Error bars indicate the mean ± s.d. * $P < 0.05$, ** $P < 0.01$, *** $P < 0.001$. (K, M, and N) One-way ANOVA and HSD *post-hoc* test. (L and O) Wilcoxon-Mann-Whitney test. Bars, 100 μm. See also Figure S4 and Table S4.

Figure 5. Effects of overexpression of target genes on class IV and requirements of Kn targets for class IV-like transformation

(A-D) Images of class IV ddaC. Control (A), *spin*-overexpression (B), *Imp*-overexpression (C), and *lola*-overexpression (D).

(E-H) Effects of knockdown of target genes on Kn misexpression-induced transformation. Images of control (E), *kn*-misexpressing (F), *kn* and *dOrai*-dsRNA expressing (G), and *kn* and *lola*-dsRNA expressing (H) class I ddaE. (I-J) Quantitative analysis. (I) Quantification of terminal numbers of the dorsal side of the ddaC arbor. (J) Quantitative analyses of the number of branch termini per cell of class I ddaE of the indicated genotypes. Most notably, knockdown of *lola* or *dOrai*

restored the class IV-like arbor to normal class I with respect to both the branch number and the comb-like shape. Error bars indicate the mean ± s.d. * $P < 0.05$, ** $P < 0.01$, *** $P < 0.001$ (one-way ANOVA and HSD *post-hoc* test). Black asterisks indicate statistically significant differences from the control (leftmost dataset), and blue asterisks from the *kn*-misexpressing neuron (the second or third from the left). NS: Statistically not significant ($P > 0.05$). Due to a technical difficulty, we were unable to address the relevance of the Ab targets in the Ab misexpression-induced context (see RNAi in SUPPLEMENTAL INFORMATION). Bars, 100 μm. See also Table S4.

Figure 6. *Ten-m* knockdown phenotypes of class I ddaE and *Ten-m* expression pattern in neuronal and non-neuronal tissues

(A-D' and M) Phenotypes of class I neuron ddaE when *Ten-m* was knocked down by using *GAL4[2-21]* (B) or *arm-GAL4* (D and D'). (A, C, and C') Controls. (C' and D') Tracings of C and D, respectively. (M) Quantitative analysis. The ratio of the number of anterior-directed secondary branches to the number of posterior-directed secondary branches was plotted. Error bars indicate the mean ± s.d. ** $P < 0.01$, *** $P < 0.001$ (Wilcoxon-Mann-Whitney test).

(E-J) *Ten-m* expression in dorsal regions in larval hemisegments. *Ten-m* expression pattern was monitored by mCD8:GFP expression under the *Ten-m-GAL4* enhancer trap line (green in E and H, and E', F, H'-J) and co-imaged with a class IV marker *ppk-CD4:tdTom* (magenta in E and H). Cell bodies of class I and IV neurons are

marked by arrowheads and arrows, respectively. Dendritic branches of class I are labeled much more intensely than those of class IV by *Ten-m-GAL4*, and the cell bodies of both classes are almost masked by strong signals of overlying epidermis (E and E'). (F) Images of ten hemisegments are overlaid with reference to cell bodies of class IV ddaC (arrow) and the signal intensity is represented by the indicated color code. (G) Quantification of mCD8:GFP signals in epidermis encompassing the cell bodies (cell-body region) and those close to branch termini of class I ddaE (terminal region). Error bars indicate the mean ± s.d. *** $P < 0.001$ (Wilcoxon-Mann-Whitney test). (H and H') High-power images of proximal dendritic regions of ddaE and class IV ddaC. In contrast to ddaE branches that were strongly labeled by *Ten-m GAL4*, *ppk-CD4:tdTom*-positive branches of ddaC were only weakly visualized by *Ten-m GAL4* (arrows). (I and J) Decrease in *Ten-m* expression level in an *ab* mutant larva (24-26 hr AEL). Cell bodies of class I ddaD and ddaE are marked by arrowheads. Note that signals in dendrites were hardly seen in the *ab* mutant.

(K-L', M, and N) Effects of *Ten-m* overexpression in the epidermal *hh* domain on dendrite patterning of class I ddaE. (K-L') The *hh* domain was visualized by GFP expression driven by *hh-GAL4* (green) and dendrites were labeled by anti-HRP antibody (magenta). (K' and L') Tracings of K and L, respectively. (M and N) Quantitative analysis. (M) The ratio of the number of anterior-directed secondary branches to the number of posterior-directed secondary branches was plotted (GAL4: *hh*). (N) The number of branch termini in the *hh* domain. Error bars indicate

the mean ± s.d. *** $P < 0.001$ (Wilcoxon-Mann-Whitney test). Bars, 100 μm (A and B, C-D', E and E', F, H and H', and K-L'); 50 μm (I and J). See also Figure S5.

Figure 7. Effects of *Ten-m* knockdown in class IV ddaC and/or adjacent tissues on orientation distributions of its branch termini

(A-N') Images of class IV ddaC when *Ten-m* was knocked down by using *ppk-GAL4* (B, H, and H'), *Ten-m-GAL4* (D, J, and J'), or *hh-GAL4* (F, L, L', N, and N'). (A, C, E, G, G', I, I', K, K', M, and M') Controls. (G-N') High-power images of boxed areas in A-F. Orientations of branch termini are defined by short line segments, which trace termini to 5-10 mm-distant intra-branch points (G'-N'). Bars, 100 μm.

(O-V) Orientation distributions of branch termini. In each rose diagram, angles are classed into 9 bins (20° for each bin) and visualized in a point symmetry manner. (O-R) Data of individual genotypes were collected from 200mm x 200mm boxed areas in A-D. (S-T and U-V) Data were collected from dorsal *hh* domains in dendritic arbors (green zones dorsal to the cell bodies) and from the sides opposite to the *hh* domains (magenta zones dorsal to the cell bodies), respectively. Indicated at a lower left-hand corner of each rose diagram are the number of branch termini and the number of neurons from which the data were collected (in parentheses). The lengths of the mean vector (orange arrows) are indicated (r). All knockdowns tested significantly biased the orientation distribution (O and P; $P < 0.01$; Q and R; $P < 0.001$; S and T; $P < 0.001$; Mardia-Watson-Wheeler test), except for in the magenta zones (U and V).

Figure 8. An effect of *Ten-m* overexpression in class IV on directional preference of branch growth along the A-P axis

(A-D') Images of class IV ddaC (A, A', B, and B') or class I ddaE (C, C', D, and D'). Controls (A, A', C, and C') and *Ten-m*-overexpressing neurons (B, B', D, and D'). (A'-D') High-power images of 200μm x 200μm boxed areas in A-D. Anterior-directed and posterior-directed termini are indicated by magenta and green points, respectively. Bars, 100 μm. (E and F) Quantitative analyses. (E) The anterior vs. posterior directional bias in the boxed areas was quantified and statistically tested. (F) The number of termini in the boxed areas. Error bars indicate the mean ± s.d. ** $P < 0.01$, *** $P < 0.001$ (one-way ANOVA and HSD *post-hoc* test). NS: Statistically not significant ($P > 0.05$). (G) Summary of phenotypes and a hypothetical Ten-m-mediated dendrite-epidermis interaction in various genetic backgrounds. (Top) A diagram showing the non-uniform Ten-m expression profile in the epidermis. The X-axis represents the A-P axis and the Y-axis indicates the amount of Ten-m in the epidermis. An alignment of epidermal cells with a decreasing Ten-m amount is also schematized. The two epidermal cells from the origin along the X axis indicate Ten-m-high cells that encompass cell bodies of da neurons in the dorsal cluster, such as ddaC and ddaE. (Left and right) Diagrams illustrating dendrite phenotypes of class I ddaE and class IV ddaC, respectively, and hypothetical Ten-m-mediated dendrite-epidermis interactions in different genetic backgrounds. Each diagram of the dendrite phenotype represents the overall ddaE arbor (left) or the posterior half

of the ddaC arbor (right). Thick green- and magenta-outlined boxes illustrate wild-type (WT) ddaE and ddaC, respectively. (Left) Ten-m-high dendrites of WT ddaE respond to the epidermal high-low Ten-m imbalance, and sprout and extend down the lower slope, realizing the predominantly posterior-oriented comb-like pattern (arrow at the top). When the Ten-m-mediated interaction is disrupted, for example, by a cell-autonomous knockdown, dendrites no longer sense the epidermal Ten-m level, and the directional preference of the branch sprouting is abrogated (double-headed arrow at the bottom). (Right) In WT ddaC, the low-level expression in the neurons and the epidermis ensures the relatively radial pattern of terminal branches in the *hh* domain (crossed arrows in the middle). When the Ten-m-mediated interaction is abrogated, extension of terminal branches is biased along the A-P axis by an unknown mechanism (double-headed arrow at the bottom). When Ten-m is overexpressed in ddaC, its branches respond to the higher-to-lower level of epidermal Ten-m towards the posterior border in each hemisegment, as does the WT ddaE (arrow at the top).

REFERENCES

Adolph, S.K., DeLotto, R., Nielsen, F.C., and Christiansen, J. (2009). Embryonic expression of Drosophila IMP in the developing CNS and PNS. Gene expression patterns : GEP *9*, 138-143.

Agrawal, N., Venkiteswaran, G., Sadaf, S., Padmanabhan, N., Banerjee, S., and Hasan, G. (2010). Inositol 1,4,5-trisphosphate receptor and dSTIM function in Drosophila insulin-producing neurons regulates systemic intracellular calcium homeostasis and flight. J Neurosci *30*, 1301-1313.

Baumgartner, S., Martin, D., Hagios, C., and Chiquet-Ehrismann, R. (1994). Tenm, a Drosophila gene related to tenascin, is a new pair-rule gene. The EMBO journal *13*, 3728-3740.

Bertrand, N., Castro, D.S., and Guillemot, F. (2002). Proneural genes and the specification of neural cell types. Nature reviews *3*, 517-530.

Boylan, K.L., Mische, S., Li, M., Marques, G., Morin, X., Chia, W., and Hays, T.S. (2008). Motility screen identifies Drosophila IGF-II mRNA-binding protein--zipcode-binding protein acting in oogenesis and synaptogenesis. PLoS genetics *4*, e36.

Castro, D.S., Martynoga, B., Parras, C., Ramesh, V., Pacary, E., Johnston, C., Drechsel, D., Lebel-Potter, M., Garcia, L.G., Hunt, C.*, et al.* (2011). A novel function of the proneural factor Ascl1 in progenitor proliferation identified by genome-wide characterization of its targets. Genes & development *25*, 930-945.

Choksi, S.P., Southall, T.D., Bossing, T., Edoff, K., de Wit, E., Fischer, B.E., van Steensel, B., Micklem, G., and Brand, A.H. (2006). Prospero acts as a binary switch between self-renewal and differentiation in Drosophila neural stem cells. Developmental cell *11*, 775-789.

Corty, M.M., Matthews, B.J., and Grueber, W.B. (2009). Molecules and mechanisms of dendrite development in Drosophila. Development *136*, 1049-1061.

Crozatier, M., and Vincent, A. (2008). Control of multidendritic neuron differentiation in Drosophila: the role of Collier. Developmental biology *315*, 232-242.

Dalla Torre di Sanguinetto, S.A., Dasen, J.S., and Arber, S. (2008). Transcriptional mechanisms controlling motor neuron diversity and connectivity. Curr Opin Neurobiol *18*, 36-43.

Dennis, G., Jr., Sherman, B.T., Hosack, D.A., Yang, J., Gao, W., Lane, H.C., and Lempicki, R.A. (2003). DAVID: Database for Annotation, Visualization, and Integrated Discovery. Genome biology *4*, P3.

Dermaut, B., Norga, K.K., Kania, A., Verstreken, P., Pan, H., Zhou, Y., Callaerts, P., and Bellen, H.J. (2005). Aberrant lysosomal carbohydrate storage accompanies endocytic defects and neurodegeneration in Drosophila benchwarmer. The Journal of cell biology *170*, 127-139.

Dubois, L., Enriquez, J., Daburon, V., Crozet, F., Lebreton, G., Crozatier, M., and Vincent, A. (2007). Collier transcription in a single Drosophila muscle lineage: the combinatorial control of muscle identity. Development *134*, 4347-4355.

Filion, G.J., van Bemmel, J.G., Braunschweig, U., Talhout, W., Kind, J., Ward, L.D., Brugman, W., de Castro, I.J., Kerkhoven, R.M., Bussemaker, H.J*., et al.* (2010). Systematic protein location mapping reveals five principal chromatin types in Drosophila cells. Cell *143*, 212-224.

Fishell, G., and Hanashima, C. (2008). Pyramidal neurons grow up and change their mind. Neuron *57*, 333-338.

Gao, F.B., Brenman, J.E., Jan, L.Y., and Jan, Y.N. (1999). Genes regulating dendritic outgrowth, branching, and routing in Drosophila. Genes & development *13*, 2549-2561.

Giniger, E., Tietje, K., Jan, L.Y., and Jan, Y.N. (1994). lola encodes a putative transcription factor required for axon growth and guidance in Drosophila. Development *120*, 1385-1398.

Grueber, W.B., Jan, L.Y., and Jan, Y.N. (2002). Tiling of the Drosophila epidermis by multidendritic sensory neurons. Development *129*, 2867-2878.

Grueber, W.B., Jan, L.Y., and Jan, Y.N. (2003). Different levels of the homeodomain protein cut regulate distinct dendrite branching patterns of Drosophila multidendritic neurons. Cell *112*, 805-818.

Hammer, Ø., Harper, D.A.T. & Ryan, P.D. (2001). Past: paleontological statistics software package for education and data analysis. Palaeontologia Electronica *4*, 9.

Han, C., Wang, D., Soba, P., Zhu, S., Lin, X., Jan, L.Y., and Jan, Y.N. (2012). Integrins regulate repulsion-mediated dendritic patterning of drosophila sensory neurons by restricting dendrites in a 2D space. Neuron *73*, 64-78.

Hattori, Y., Sugimura, K., and Uemura, T. (2007). Selective expression of Knot/Collier, a transcriptional regulator of the EBF/Olf-1 family, endows the

Drosophila sensory system with neuronal class-specific elaborated dendritic patterns. Genes to cells : devoted to molecular & cellular mechanisms *12*, 1011-1022.

Hausser, M., and Mel, B. (2003). Dendrites: bug or feature? Curr Opin Neurobiol *13*, 372-383.

Hobert, O., Carrera, I., and Stefanakis, N. (2010). The molecular and gene regulatory signature of a neuron. Trends in neurosciences *33*, 435-445.

Hong, W., Mosca, T.J., and Luo, L. (2012). Teneurins instruct synaptic partner matching in an olfactory map. Nature *484*, 201-207.

Hu, S., Fambrough, D., Atashi, J.R., Goodman, C.S., and Crews, S.T. (1995). The Drosophila abrupt gene encodes a BTB-zinc finger regulatory protein that controls the specificity of neuromuscular connections. Genes & development *9*, 2936-2948.

Huang da, W., Sherman, B.T., and Lempicki, R.A. (2009). Systematic and integrative analysis of large gene lists using DAVID bioinformatics resources. Nature protocols *4*, 44-57.

Im, S.H., and Galko, M.J. (2012). Pokes, sunburn, and hot sauce: Drosophila as an emerging model for the biology of nociception. Dev Dyn *241*, 16-26.

Iyer, E.P., Iyer, S.C., Sulkowski, M.J., and Cox, D.N. (2009). Isolation and purification of Drosophil peripheral neurons by magnetic bead sorting. J Vis Exp.

Jan, Y.N., and Jan, L.Y. (2003). The control of dendrite development. Neuron *40*, 229-242.

Jan, Y.N., and Jan, L.Y. (2010). Branching out: mechanisms of dendritic arborization. Nature reviews *11*, 316-328.

Jinushi-Nakao, S., Arvind, R., Amikura, R., Kinameri, E., Liu, A.W., and Moore, A.W. (2007). Knot/Collier and cut control different aspects of dendrite cytoskeleton and synergize to define final arbor shape. Neuron *56*, 963-978.

Kharchenko, P.V., Alekseyenko, A.A., Schwartz, Y.B., Minoda, A., Riddle, N.C., Ernst, J., Sabo, P.J., Larschan, E., Gorchakov, A.A., Gu, T.*, et al.* (2010). Comprehensive analysis of the chromatin landscape in Drosophila melanogaster. Nature *471*, 480-485.

Kim, M.E., Shrestha, B.R., Blazeski, R., Mason, C.A., and Grueber, W.B. (2012). Integrins establish dendrite-substrate relationships that promote dendritic self-avoidance and patterning in drosophila sensory neurons. Neuron *73*, 79-91.

Landgraf, M., and Evers, J.F. (2005). Control of dendritic diversity. Current opinion in cell biology *17*, 690-696.

Leamey, C.A., Merlin, S., Lattouf, P., Sawatari, A., Zhou, X., Demel, N., Glendining, K.A., Oohashi, T., Sur, M., and Fassler, R. (2007). Ten_m3 regulates eye-specific patterning in the mammalian visual pathway and is required for binocular vision. PLoS biology *5*, e241.

Levine, A., Bashan-Ahrend, A., Budai-Hadrian, O., Gartenberg, D., Menasherow, S., and Wides, R. (1994). Odd Oz: a novel Drosophila pair rule gene. Cell *77*, 587-598.

Li, W., Wang, F., Menut, L., and Gao, F.B. (2004). BTB/POZ-zinc finger protein abrupt suppresses dendritic branching in a neuronal subtype-specific and dosage-dependent manner. Neuron *43*, 823-834.

London, M., and Hausser, M. (2005). Dendritic computation. Annu Rev Neurosci *28*, 503-532.

Long, H., Ou, Y., Rao, Y., and van Meyel, D.J. (2009). Dendrite branching and self-avoidance are controlled by Turtle, a conserved IgSF protein in Drosophila. Development *136*, 3475-3484.

Matsubara, D., Horiuchi, S.Y., Shimono, K., Usui, T., and Uemura, T. The seven-pass transmembrane cadherin Flamingo controls dendritic self-avoidance via its binding to a LIM domain protein, Espinas, in Drosophila sensory neurons. Genes & development *25*, 1982-1996.

McQuilton, P., St Pierre, S.E., and Thurmond, J. (2012). FlyBase 101--the basics of navigating FlyBase. Nucleic acids research *40*, D706-714.

Mosca, T.J., Hong, W., Dani, V.S., Favaloro, V., and Luo, L. (2012). Trans-synaptic Teneurin signalling in neuromuscular synapse organization and target choice. Nature *484*, 237-241.

Negre, N., Brown, C.D., Ma, L., Bristow, C.A., Miller, S.W., Wagner, U., Kheradpour, P., Eaton, M.L., Loriaux, P., Sealfon, R.*, et al.* (2011). A cis-regulatory map of the Drosophila genome. Nature *471*, 527-531.

Parrish, J.Z., Emoto, K., Jan, L.Y., and Jan, Y.N. (2007). Polycomb genes interact with the tumor suppressor genes hippo and warts in the maintenance of Drosophila sensory neuron dendrites. Genes & development *21*, 956-972.

Parrish, J.Z., Kim, M.D., Jan, L.Y., and Jan, Y.N. (2006). Genome-wide analyses identify transcription factors required for proper morphogenesis of Drosophila sensory neuron dendrites. Genes & development *20*, 820-835.

Parrish, J.Z., Xu, P., Kim, C.C., Jan, L.Y., and Jan, Y.N. (2009). The microRNA bantam functions in epithelial cells to regulate scaling growth of dendrite arbors in drosophila sensory neurons. Neuron *63*, 788-802.

Satoh, D., Sato, D., Tsuyama, T., Saito, M., Ohkura, H., Rolls, M.M., Ishikawa, F., and Uemura, T. (2008). Spatial control of branching within dendritic arbors by dynein-dependent transport of Rab5-endosomes. Nature cell biology *10*, 1164-1171.

Schwartz, Y.B., Kahn, T.G., Stenberg, P., Ohno, K., Bourgon, R., and Pirrotta, V. (2010). Alternative epigenetic chromatin states of polycomb target genes. PLoS genetics *6*, e1000805.

Shimono, K., Fujimoto, A., Tsuyama, T., Yamamoto-Kochi, M., Sato, M., Hattori, Y., Sugimura, K., Usui, T., Kimura, K., and Uemura, T. (2009). Multidendritic sensory neurons in the adult Drosophila abdomen: origins, dendritic morphology, and segment- and age-dependent programmed cell death. Neural development *4*, 37.

Southall, T.D., and Brand, A.H. (2009). Neural stem cell transcriptional networks highlight genes essential for nervous system development. The EMBO journal *28*, 3799-3807.

Spletter, M.L., Liu, J., Liu, J., Su, H., Giniger, E., Komiyama, T., Quake, S., and Luo, L. (2007). Lola regulates Drosophila olfactory projection neuron identity and targeting specificity. Neural development *2*, 14.

Sugimura, K., Satoh, D., Estes, P., Crews, S., and Uemura, T. (2004). Development of morphological diversity of dendrites in Drosophila by the BTB-zinc finger protein abrupt. Neuron *43*, 809-822.

Sugino, K., Hempel, C.M., Miller, M.N., Hattox, A.M., Shapiro, P., Wu, C., Huang, Z.J., and Nelson, S.B. (2006). Molecular taxonomy of major neuronal classes in the adult mouse forebrain. Nature neuroscience *9*, 99-107.

Sweeney, S.T., and Davis, G.W. (2002). Unrestricted synaptic growth in spinster-a late endosomal protein implicated in TGF-beta-mediated synaptic growth regulation. Neuron *36*, 403-416.

van Steensel, B., Delrow, J., and Henikoff, S. (2001). Chromatin profiling using targeted DNA adenine methyltransferase. Nature genetics *27*, 304-308.

van Steensel, B., and Henikoff, S. (2000). Identification of in vivo DNA targets of chromatin proteins using tethered dam methyltransferase. Nat Biotechnol *18*, 424-428.

Venkiteswaran, G., and Hasan, G. (2009). Intracellular Ca2+ signaling and store-operated Ca2+ entry are required in Drosophila neurons for flight. Proceedings of the National Academy of Sciences of the United States of America *106*, 10326-10331.

Vrieseling, E., and Arber, S. (2006). Target-induced transcriptional control of dendritic patterning and connectivity in motor neurons by the ETS gene Pea3. Cell *127*, 1439-1452.

Yamamoto, M., Ueda, R., Takahashi, K., Saigo, K., and Uemura, T. (2006). Control of axonal sprouting and dendrite branching by the Nrg-Ank complex at the neuron-glia interface. Curr Biol *16*, 1678-1683.

Ye, B., Zhang, Y., Song, W., Younger, S.H., Jan, L.Y., and Jan, Y.N. (2007). Growing dendrites and axons differ in their reliance on the secretory pathway. Cell *130*, 717-729.

Yisraeli, J.K. (2005). VICKZ proteins: a multi-talented family of regulatory RNA-binding proteins. Biology of the cell / under the auspices of the European Cell Biology Organization *97*, 87-96.

Young, T.R., and Leamey, C.A. (2009). Teneurins: important regulators of neural circuitry. The international journal of biochemistry & cell biology *41*, 990-993.

Zheng, L., Michelson, Y., Freger, V., Avraham, Z., Venken, K.J., Bellen, H.J., Justice, M.J., and Wides, R. (2011). Drosophila Ten-m and filamin affect motor neuron growth cone guidance. PloS one *6*, e22956.

Zheng, Y., Josefowicz, S.Z., Kas, A., Chu, T.T., Gavin, M.A., and Rudensky, A.Y. (2007). Genome-wide analysis of Foxp3 target genes in developing and mature regulatory T cells. Nature *445*, 936-940.

Zheng, Y., Wildonger, J., Ye, B., Zhang, Y., Kita, A., Younger, S.H., Zimmerman, S., Jan, L.Y., and Jan, Y.N. (2008). Dynein is required for polarized dendritic transport and uniform microtubule orientation in axons. Nature cell biology *10*, 1172-1180.

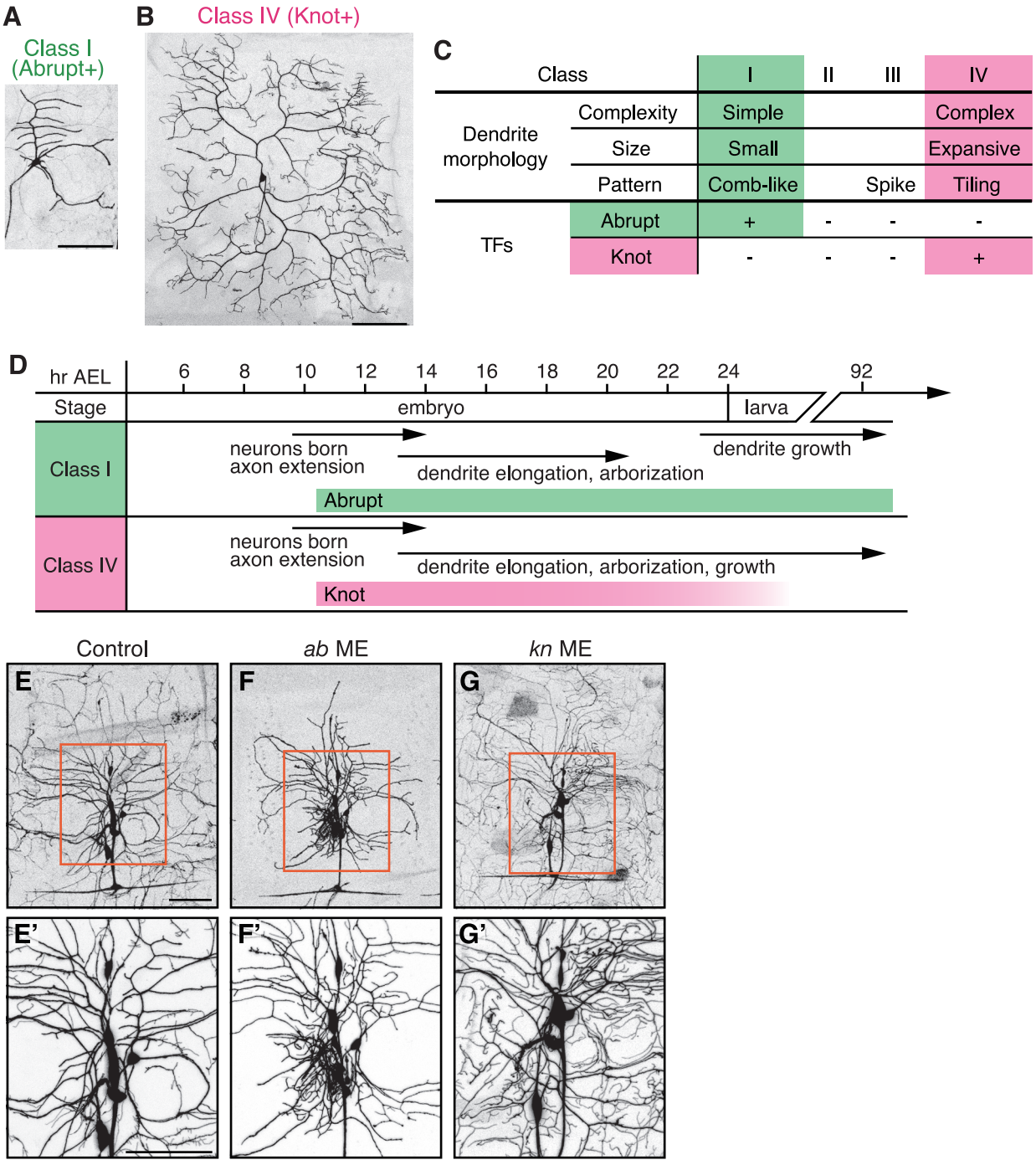
A
Class I
(Abrupt+)
B
Class IV (Knot+)
C
Class
I
II
III
IV
Dendrite morphology
Complexity
Simple
Complex
Size
Small
Expansive
Pattern
Comb-like
Spike
Tiling
TFs
Abrupt
+
-
-
-
Knot
-
-
-
+
D
hr AEL
6
8
10
12
14
16
18
20
22
24
92
Stage
embryo
larva
Class I
neurons born
axon extension
dendrite elongation, arborization
dendrite growth
Abrupt
Class IV
neurons born
axon extension
dendrite elongation, arborization, growth
Knot
Control
ab ME
kn ME
E
F
G
E'
F'
G'

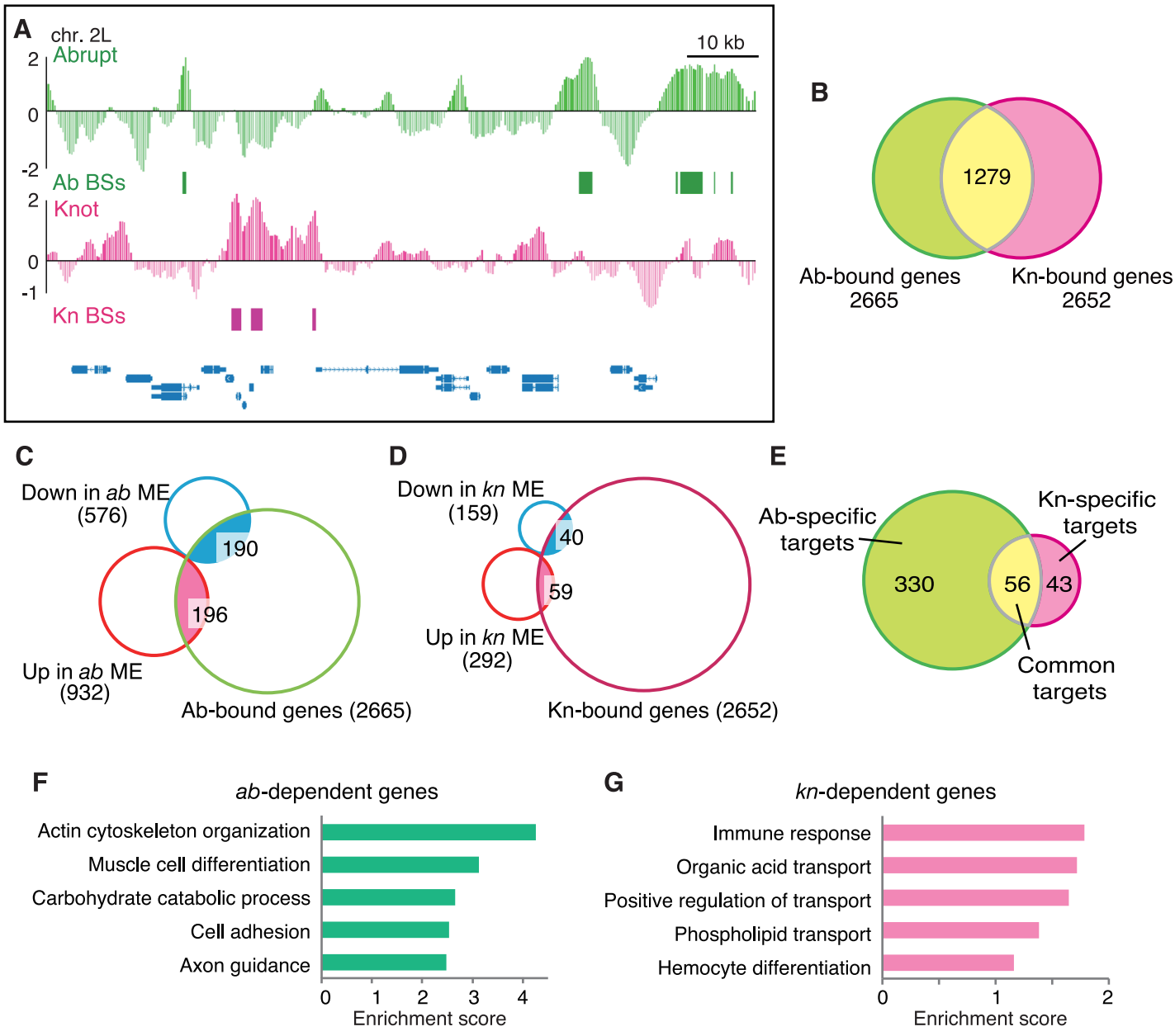
A
chr. 2L
10 kb
Abrupt
2
0
-2
Ab BSs
Knot
2
0
-1
Kn BSs
B
1279
Ab-bound genes
2665
Kn-bound genes
2652
C
Down in ab ME
(576)
190
196
Up in ab ME
(932)
Ab-bound genes (2665)
D
Down in kn ME
(159)
40
59
Up in kn ME
(292)
Kn-bound genes (2652)
E
Ab-specific
targets
Kn-specific
targets
330
56
43
Common
targets
F
ab-dependent genes
Actin cytoskeleton organization
Muscle cell differentiation
Carbohydrate catabolic process
Cell adhesion
Axon guidance
0
1
2
3
4
Enrichment score
G
kn-dependent genes
Immune response
Organic acid transport
Positive regulation of transport
Phospholipid transport
Hemocyte differentiation
0
1
2
Enrichment score

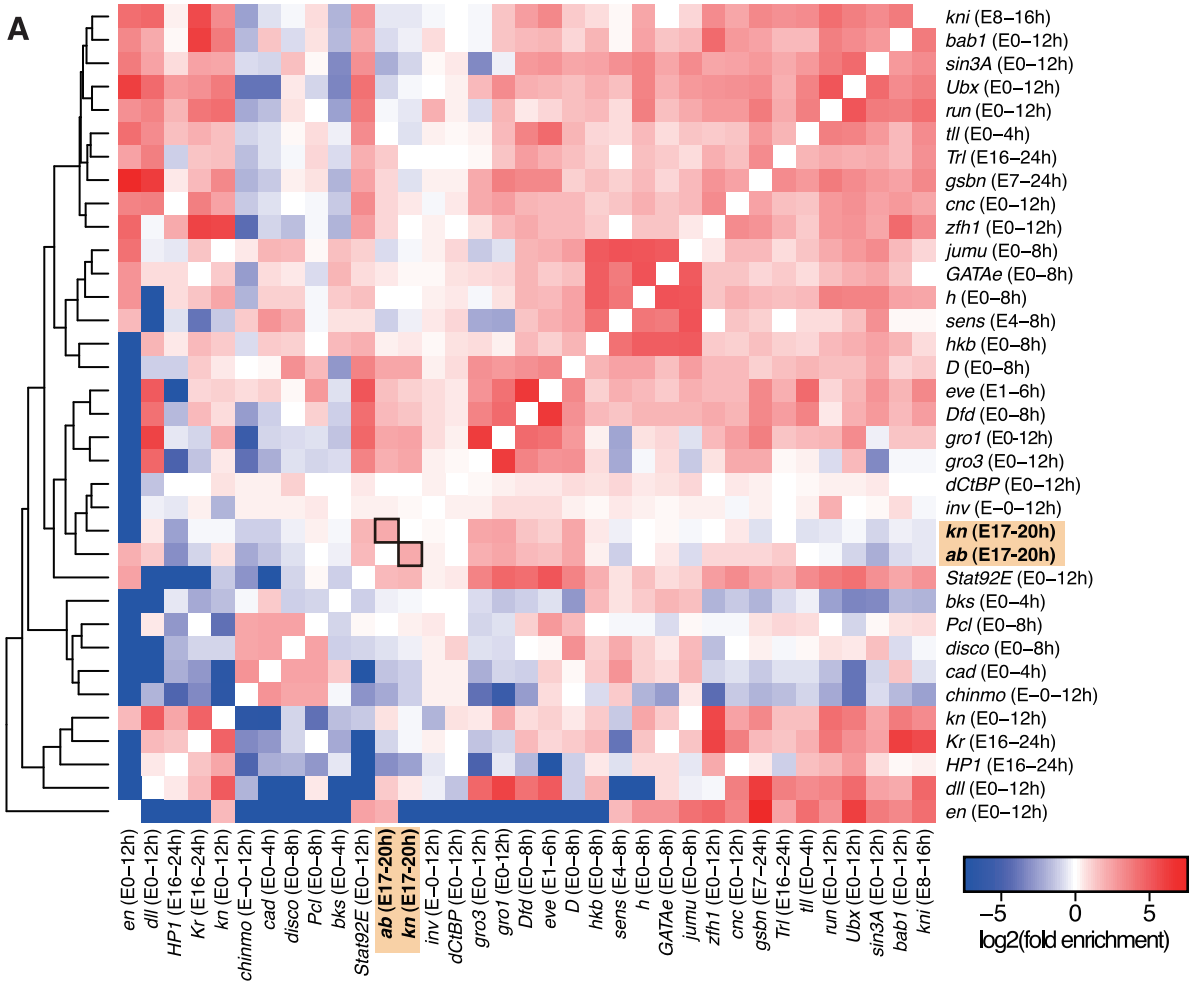
A
kni (E8–16h)
bab1 (E0–12h)
sin3A (E0–12h)
Ubx (E0–12h)
run (E0–12h)
tll (E0–4h)
Trl (E16–24h)
gsbn (E7–24h)
cnc (E0–12h)
zfh1 (E0–12h)
jumu (E0–8h)
GATAe (E0–8h)
h (E0–8h)
sens (E4–8h)
hkb (E0–8h)
D (E0–8h)
eve (E1–6h)
Dfd (E0–8h)
gro1 (E0-12h)
gro3 (E0–12h)
dCtBP (E0–12h)
inv (E–0–12h)
kn (E17-20h)
ab (E17-20h)
Stat92E (E0–12h)
bks (E0–4h)
Pcl (E0–8h)
disco (E0–8h)
cad (E0–4h)
chinmo (E–0–12h)
kn (E0–12h)
Kr (E16–24h)
HP1 (E16–24h)
dll (E0–12h)
en (E0–12h)
en (E0–12h)
dll (E0–12h)
HP1 (E16–24h)
Kr (E16–24h)
kn (E0–12h)
chinmo (E–0–12h)
cad (E0–4h)
disco (E0–8h)
Pcl (E0–8h)
bks (E0–4h)
Stat92E (E0–12h)
ab (E17-20h)
kn (E17-20h)
inv (E–0–12h)
dCtBP (E0–12h)
gro3 (E0–12h)
gro1 (E0-12h)
Dfd (E0–8h)
eve (E1–6h)
D (E0–8h)
hkb (E0–8h)
sens (E4–8h)
h (E0–8h)
GATAe (E0–8h)
jumu (E0–8h)
zfh1 (E0–12h)
cnc (E0–12h)
gsbn (E7–24h)
Trl (E16–24h)
tll (E0–4h)
run (E0–12h)
Ubx (E0–12h)
sin3A (E0–12h)
bab1 (E0–12h)
kni (E8–16h)
–5
0
5
log2(fold enrichment)
B
Ab-bound genes
Regulation of transcription
Post-embryonic organ development
Sensory organ development
Pattern specification process
Neuron differentiation
Cell motion
Tissue morphogenesis
Mesoderm development
Organ formation
Leg disc development
0
10
20
30
- log(p-value)
C
Kn-bound genes
Post-embryonic organ development
Cell motion
Sensory organ development
Neuron differentiation
Regulation of transcription
Tissue morphogenesis
Morphogenesis of an epithelium
Leg disc development
Organ formation
Cell adhesion
0
10
20
30
- log(p-value)
D
Chromatin types
1.0
0.8
0.6
0.4
0.2
0
Fraction of types
RED
YELLOW
BLACK
BLUE
GREEN
Genome
All
Up
Down
All
Up
Down
All
Up
Down
Ab BSs
Kn BSs
Pros BSs
E
RED
YELLOW
BLACK
BLUE
GREEN
All
Up
Down
All
Up
Down
All
Up
Down
Ab BSs
Kn BSs
Pros BSs
log2(fold enrichment)
–2
0
2

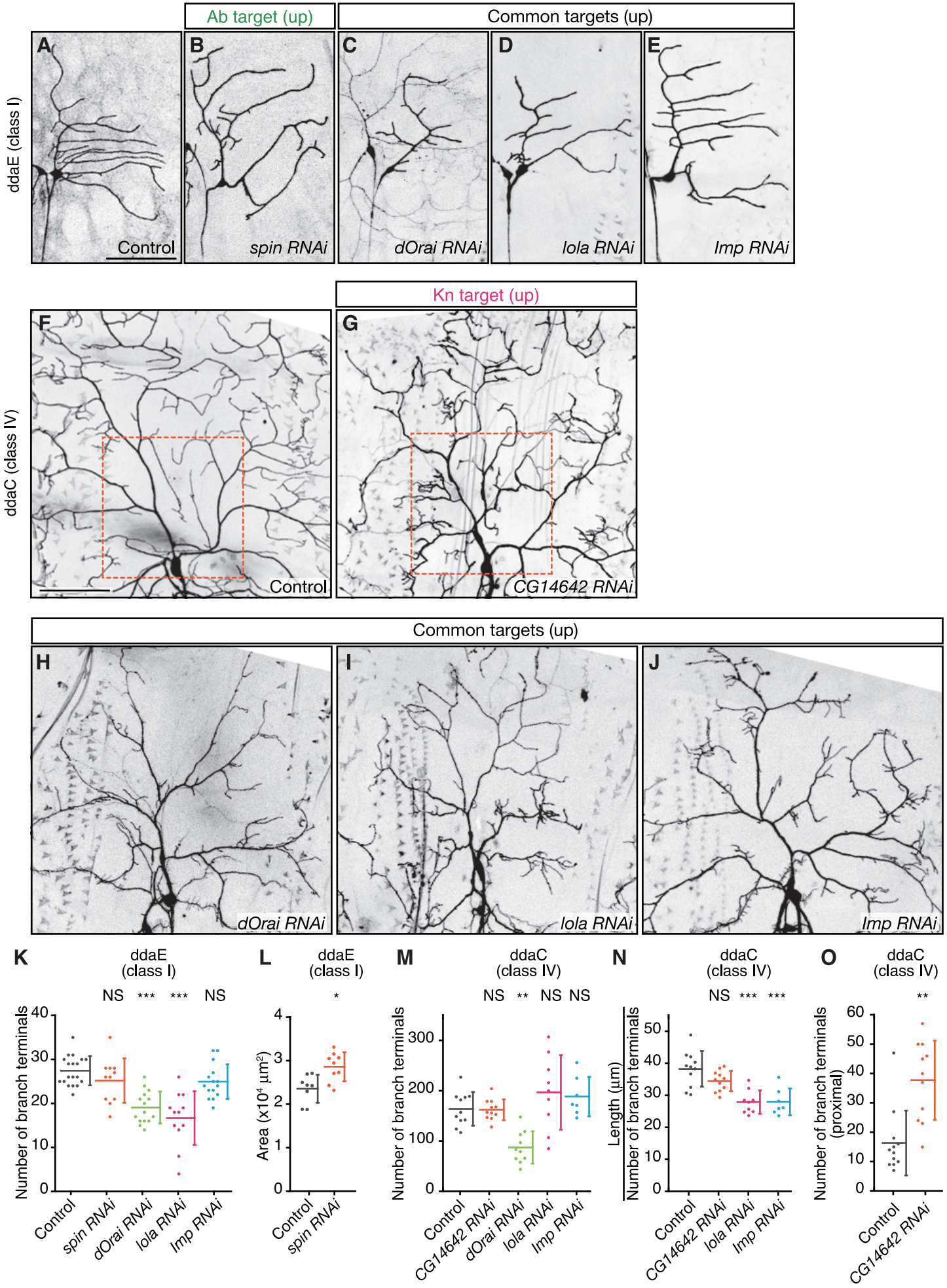
Ab target (up)
Common targets (up)
ddaE (class I)
A
Control
B
spin RNAi
C
dOrai RNAi
D
Iola RNAi
E
Imp RNAi
Kn target (up)
ddaC (class IV)
F
Control
G
CG14642 RNAi
Common targets (up)
H
dOrai RNAi
I
Iola RNAi
J
Imp RNAi
K
ddaE (class I)
NS *** *** NS
Number of branch terminals
Control
spin RNAi
dOrai RNAi
Iola RNAi
Imp RNAi
L
ddaE (class I)
*
Area (x10⁴ µm²)
Control
spin RNAi
M
ddaC (class IV)
NS ** NS NS
Number of branch terminals
Control
CG14642 RNAi
dOrai RNAi
Iola RNAi
Imp RNAi
N
ddaC (class IV)
NS *** ***
Length (µm)
Number of branch terminals
Control
CG14642 RNAi
Iola RNAi
Imp RNAi
O
ddaC (class IV)
**
Number of branch terminals (proximal)
Control
CG14642 RNAi

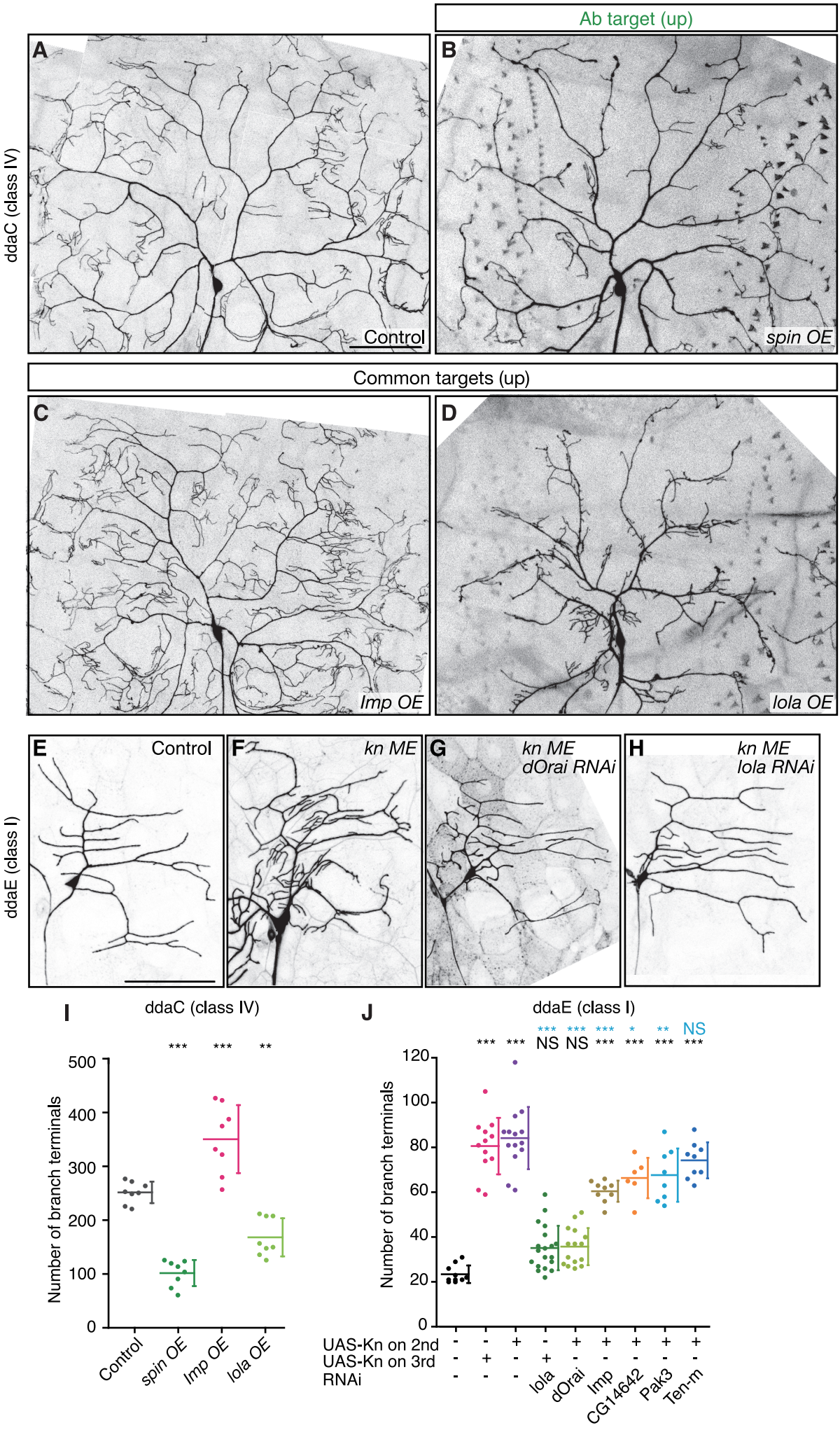
Ab target (up)
A
B
ddaC (class IV)
Control
spin OE
Common targets (up)
C
D
Imp OE
lola OE
E
F
G
H
ddaE (class I)
Control
kn ME
kn ME
dOrai RNAi
kn ME
lola RNAi
I
ddaC (class IV)
Number of branch terminals
Control
spin OE
Imp OE
lola OE
J
ddaE (class I)
Number of branch terminals
UAS-Kn on 2nd
UAS-Kn on 3rd
RNAi
lola
dOrai
Imp
CG14642
Pak3
Ten-m

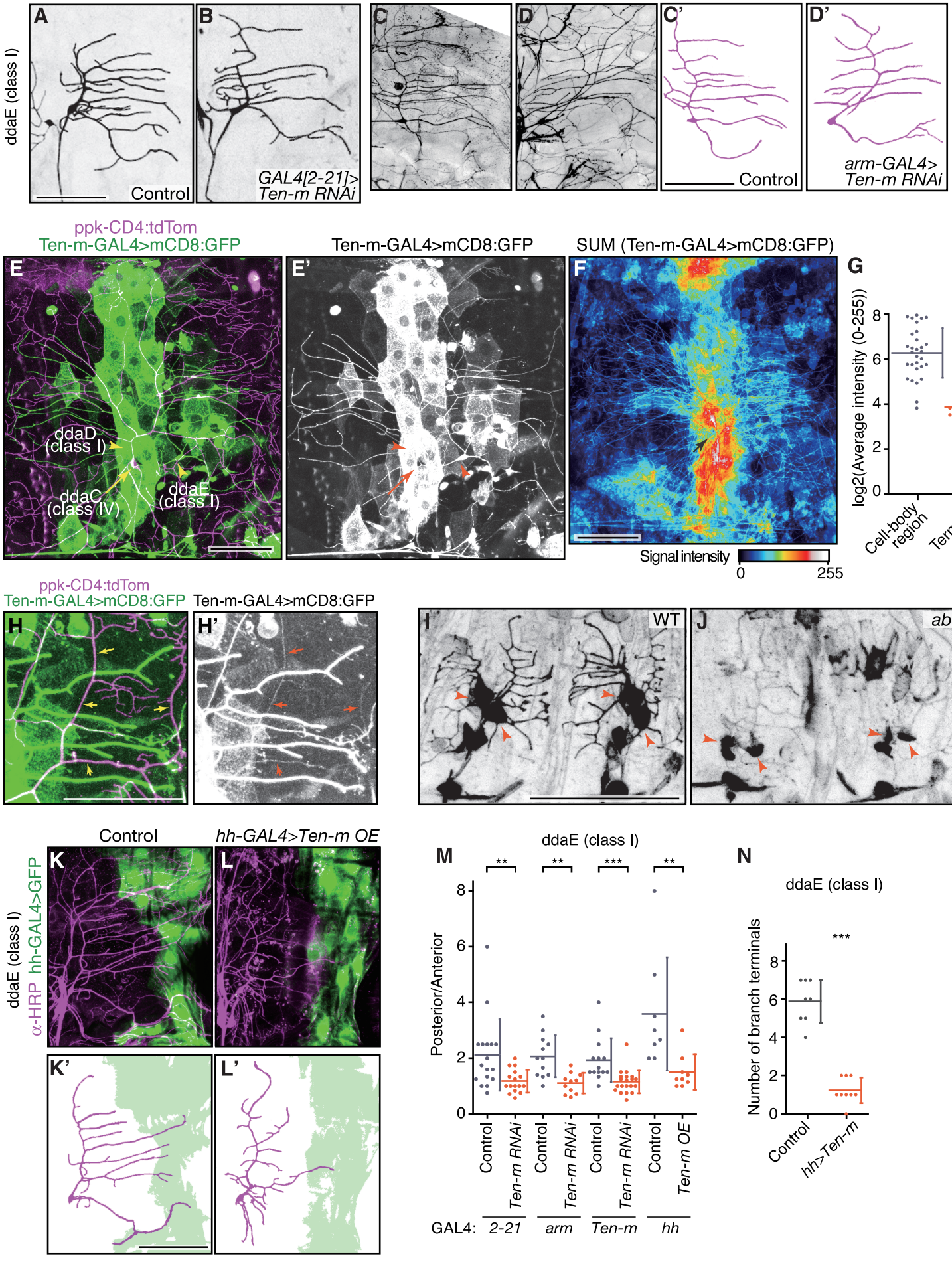
ddaE (class I)
A
Control
B
GAL4[2-21]>
Ten-m RNAi
C
D
C'
Control
D'
arm-GAL4>
Ten-m RNAi
ppk-CD4:tdTom
Ten-m-GAL4>mCD8:GFP
E
ddaD
(class I)
ddaC
(class IV)
ddaE
(class I)
Ten-m-GAL4>mCD8:GFP
E'
SUM (Ten-m-GAL4>mCD8:GFP)
F
Signal intensity
0
255
G
***
log2(Average intensity (0-255))
Cell-body region
Terminal region
ppk-CD4:tdTom
Ten-m-GAL4>mCD8:GFP
H
Ten-m-GAL4>mCD8:GFP
H'
I
WT
J
ab
Control
hh-GAL4>Ten-m OE
ddaE (class I)
α-HRP hh-GAL4>GFP
K
L
K'
L'
M
ddaE (class I)
**
**
***
**
Posterior/Anterior
Control
Ten-m RNAi
Control
Ten-m RNAi
Control
Ten-m RNAi
Control
Ten-m OE
GAL4:
2-21
arm
Ten-m
hh
N
ddaE (class I)
***
Number of branch terminals
Control
hh>Ten-m

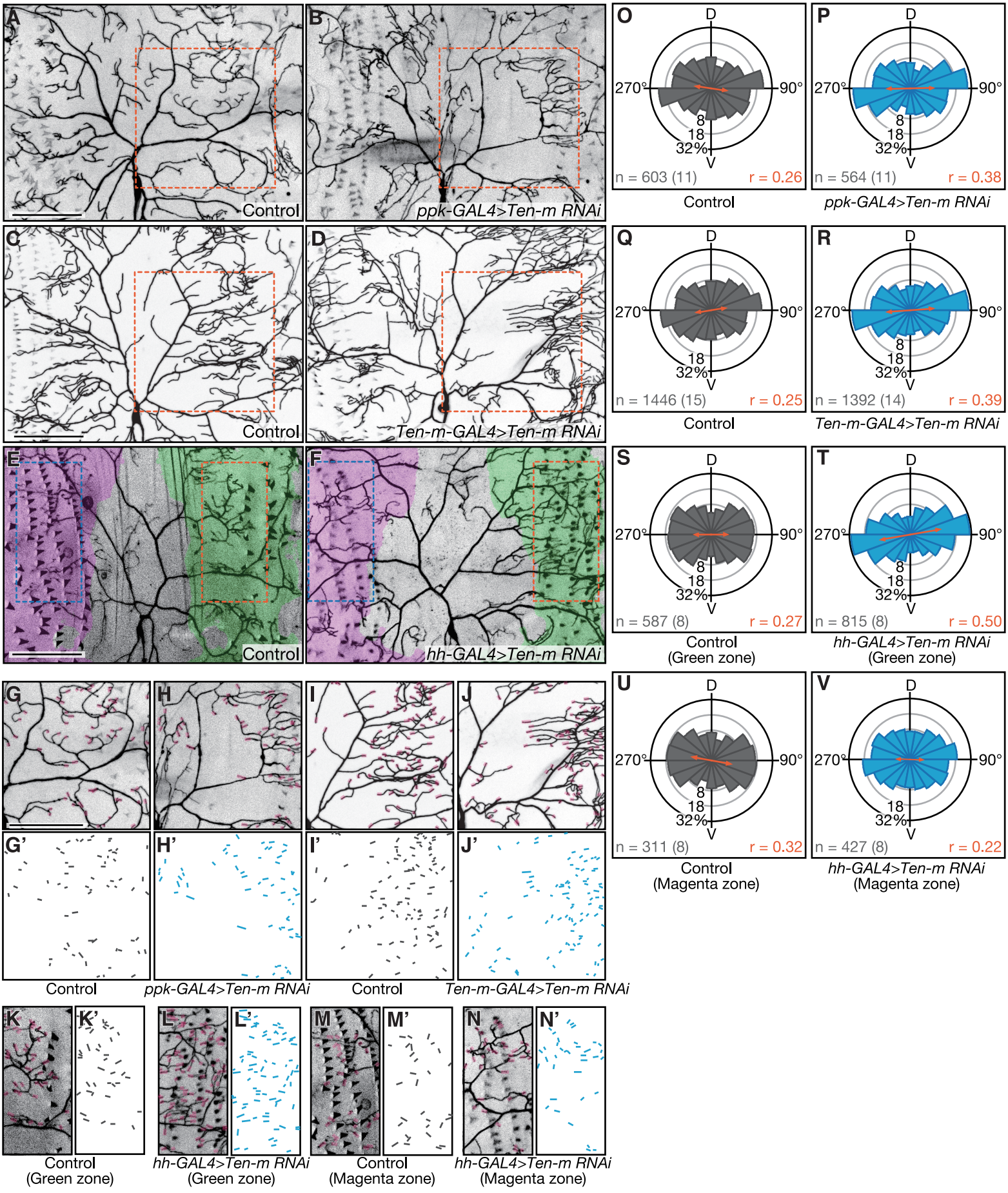
A
Control
B
ppk-GAL4>Ten-m RNAi
C
Control
D
Ten-m-GAL4>Ten-m RNAi
E
Control
F
hh-GAL4>Ten-m RNAi
G
H
I
J
G'
H'
I'
J'
Control
ppk-GAL4>Ten-m RNAi
Control
Ten-m-GAL4>Ten-m RNAi
K
K'
L
L'
M
M'
N
N'
Control
(Green zone)
hh-GAL4>Ten-m RNAi
(Green zone)
Control
(Magenta zone)
hh-GAL4>Ten-m RNAi
(Magenta zone)
O
D
270°
90°
8
18
32%
V
n = 603 (11)
r = 0.26
Control
P
D
270°
90°
8
18
32%
V
n = 564 (11)
r = 0.38
ppk-GAL4>Ten-m RNAi
Q
D
270°
90°
18
32%
V
n = 1446 (15)
r = 0.25
Control
R
D
270°
90°
8
18
32%
V
n = 1392 (14)
r = 0.39
Ten-m-GAL4>Ten-m RNAi
S
D
270°
90°
8
18
32%
V
n = 587 (8)
r = 0.27
Control
(Green zone)
T
D
270°
90°
8
18
32%
V
n = 815 (8)
r = 0.50
hh-GAL4>Ten-m RNAi
(Green zone)
U
D
270°
90°
8
18
32%
V
n = 311 (8)
r = 0.32
Control
(Magenta zone)
V
D
270°
90°
18
32%
V
n = 427 (8)
r = 0.22
hh-GAL4>Ten-m RNAi
(Magenta zone)

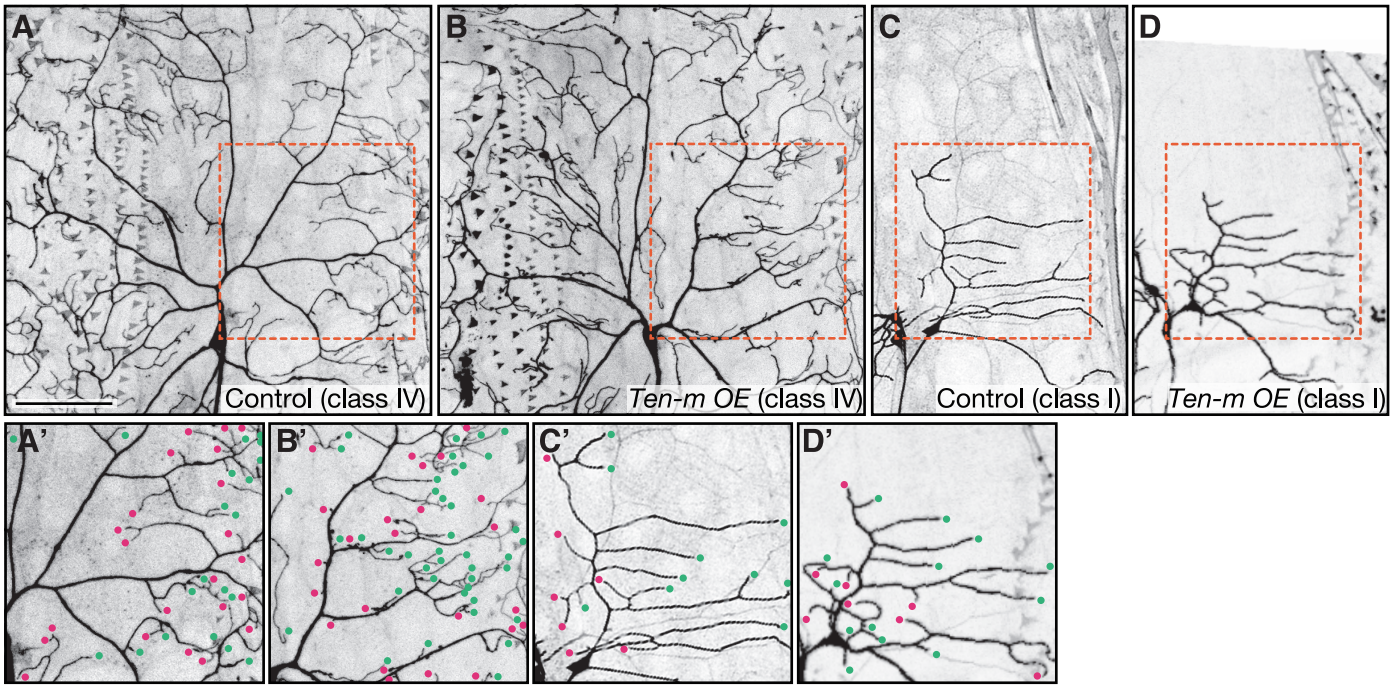
A
Control (class IV)
B
Ten-m OE (class IV)
C
Control (class I)
D
Ten-m OE (class I)
A'
B'
C'
D'

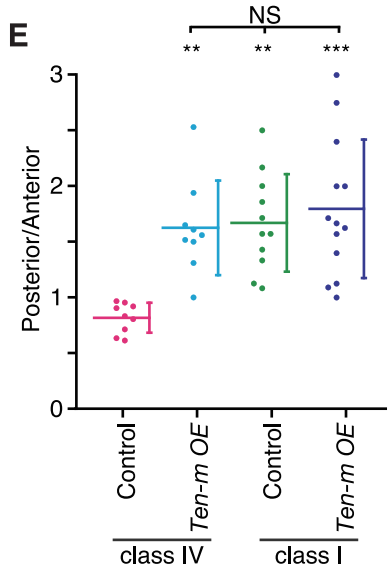
E
NS
**
**
***
Posterior/Anterior
3
2
1
0
Control
Ten-m OE
Control
Ten-m OE
class IV
class I

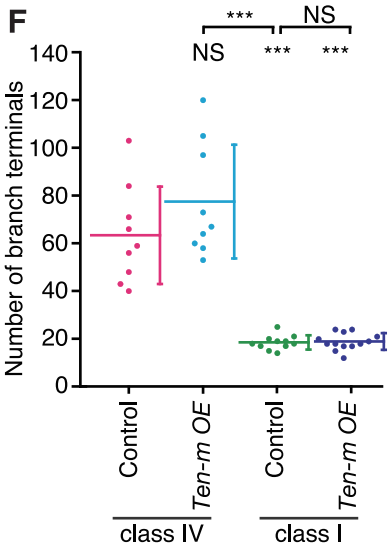
F
***
NS
NS
***
***
Number of branch terminals
140
120
100
80
60
40
20
0
Control
Ten-m OE
Control
Ten-m OE
class IV
class I

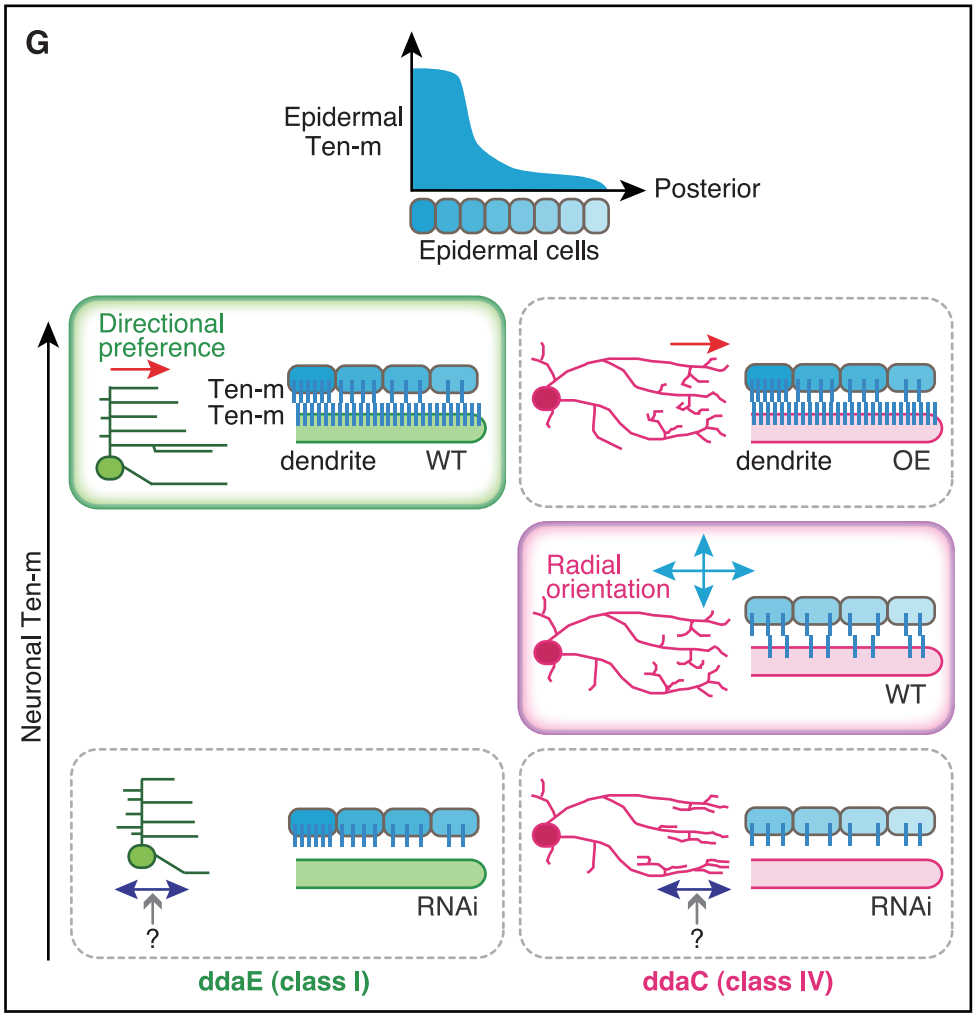
G
Epidermal Ten-m
Posterior
Epidermal cells
Neuronal Ten-m
Directional preference
Ten-m
Ten-m
dendrite
WT
dendrite
OE
Radial orientation
WT
?
RNAi
?
RNAi
ddaE (class I)
ddaC (class IV)

Inventory of Supplemental Information

1. Supplemental Figures

2. Supplemental Tables

phenotypes of either class I and/or IV when knocked down

3. Supplemental Experimental Procedures

4. Supplemental References

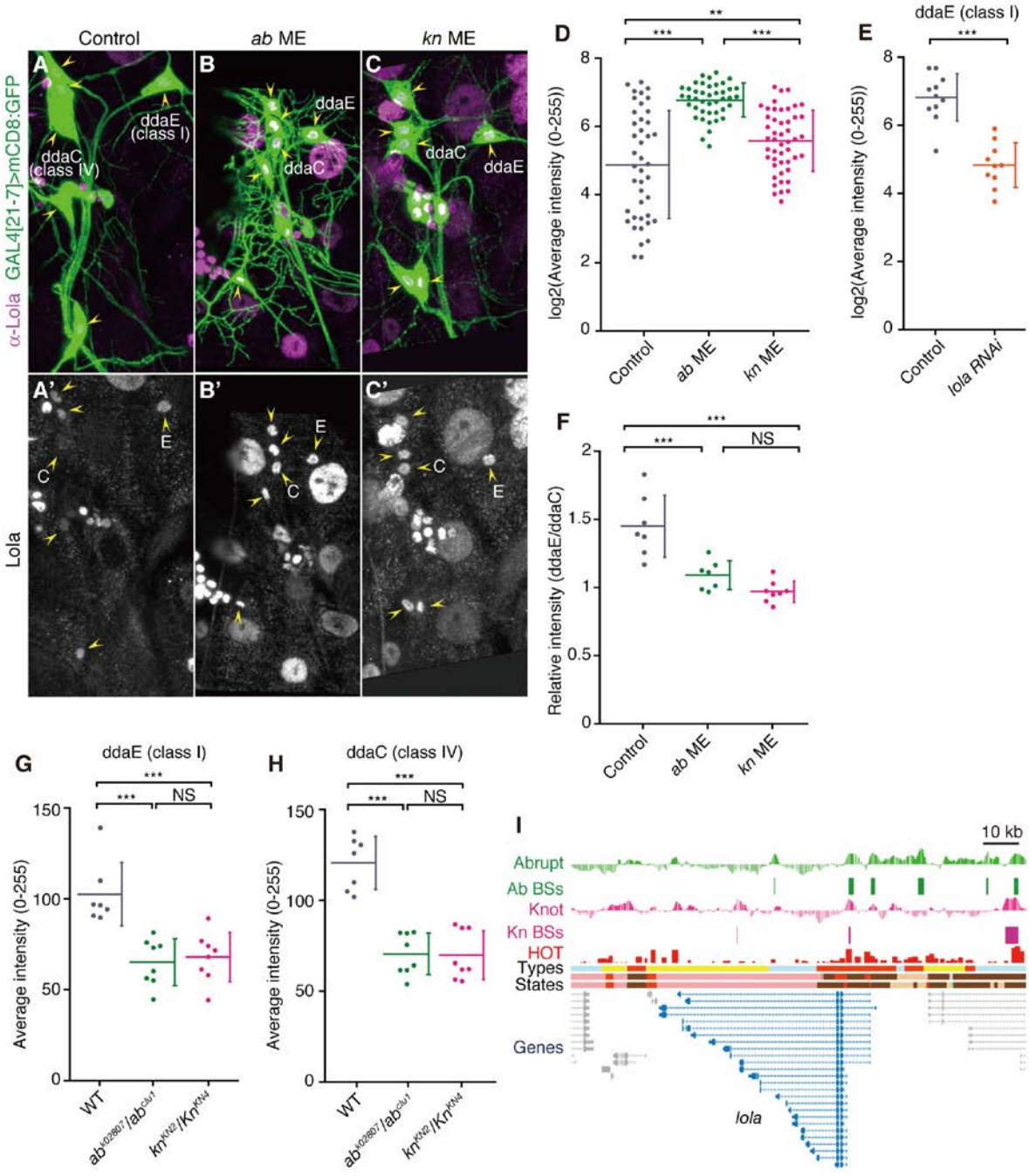

Figure S1 (Related to Figure 1). Lola levels under ME or loss of function of *ab* or *kn*

(A-E) Elevated antibody staining for the product of a common target gene *lola* under *ab* ME and *kn* ME conditions. Representative images of the staining in the control (A, A'), *ab* ME (B, B'), and *kn* ME (C, C') da neurons in wandering larvae. Images of the marker GFP (green in A, B, and C) and Lola (magenta in A, B, and C; A', B', and C'). Nuclei and cell bodies of da neurons are indicated by yellow arrowheads. *ab* ME downsizes dendritic arbors of class II-IV da neurons (Li et al., 2004; Sugimura et al., 2004), increasing the density of branches in the region proximal to the cell bodies (see Figure 1F and 1F'). (D) The elevation of the Lola signal was validated by statistical analysis of log2-transformed signal intensities of immunostaining. ** $P < 0.01$, *** $P < 0.001$ (one-way ANOVA and HSD *post-hoc* test). The distribution of the intensity was broader in the control neurons than in the ME neurons, and we wondered whether this might be due to differential expression of Lola between the da classes. (F) In fact, the Lola signal in class IV ddaC was significantly weaker than in the class I ddaE control, as shown by the ratios of signal intensity of ddaE to that of ddaC in the same hemisegment. (E) Knockdown of *lola* was confirmed by the reduced immunohistochemical signals in ddaE.

(G-H) The Lola signal of class I ddaE (G) or class IV ddaC (H) in *ab* or *kn* mutants was significantly weaker than that in the wild-type embryos. ** $P < 0.01$, *** $P < 0.001$ (one-way ANOVA and HSD *post-hoc* test). The wild-type, ab^{k02807}/ab^{clu1} or kn^{KN2}/kn^{KN4} embryos were stained for Lola and a pan-neuronal marker Elav. The level of Lola, but not Elav, was reduced in the mutants (data not shown).

(I) TF binding profiles and chromatin signatures around *lola.* DamID profiles of Ab or Kn, distributions of Ab BSs, Kn BSs, and HOT regions, chromatin types, chromatin states, and genes near *lola*.

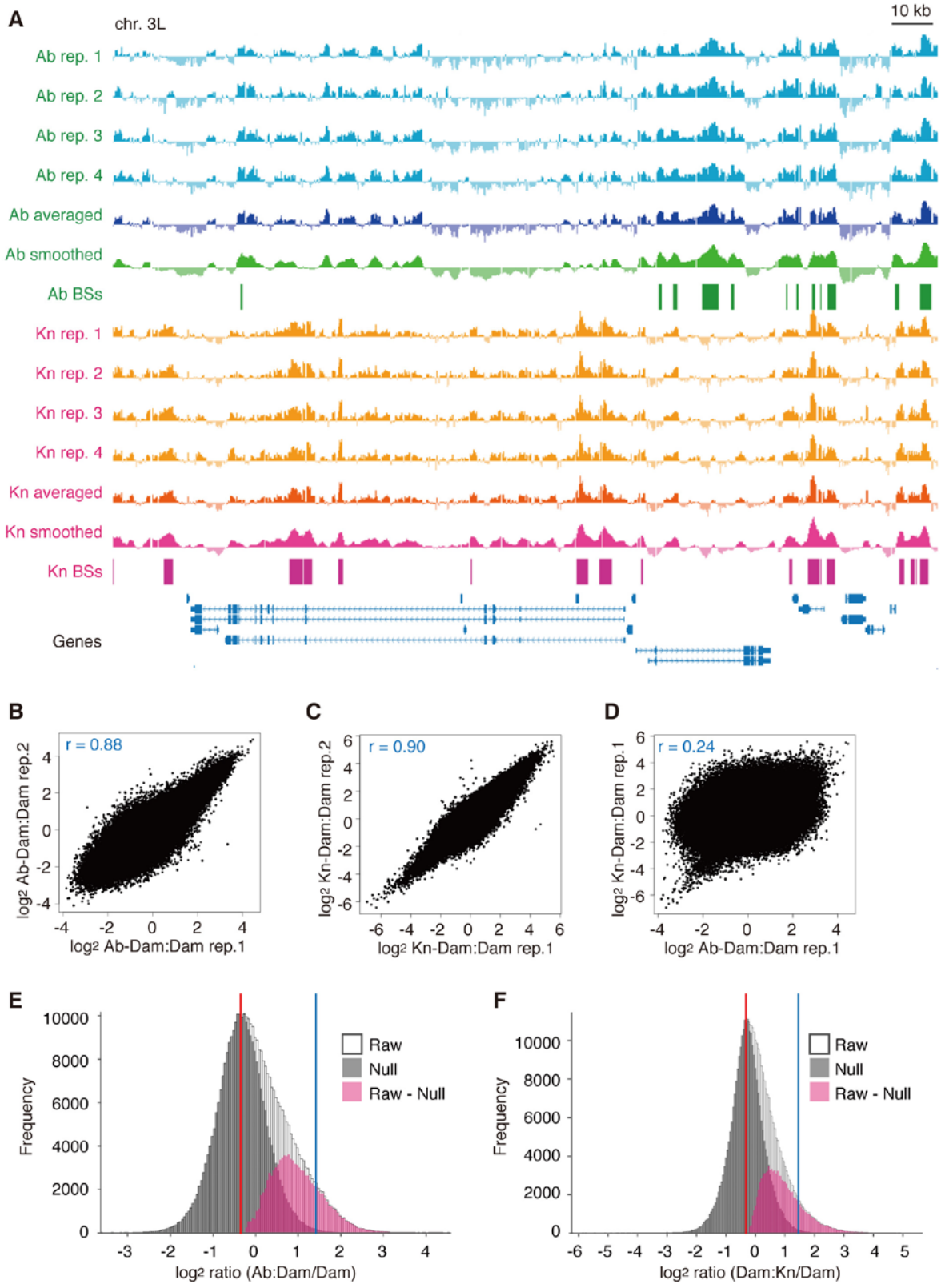
A
chr. 3L
10 kb
Ab rep. 1
Ab rep. 2
Ab rep. 3
Ab rep. 4
Ab averaged
Ab smoothed
Ab BSs
Kn rep. 1
Kn rep. 2
Kn rep. 3
Kn rep. 4
Kn averaged
Kn smoothed
Kn BSs
Genes
B
r = 0.88
log2 Ab-Dam:Dam rep.2
log2 Ab-Dam:Dam rep.1
C
r = 0.90
log2 Kn-Dam:Dam rep.2
log2 Kn-Dam:Dam rep.1
D
r = 0.24
log2 Kn-Dam:Dam rep.1
log2 Ab-Dam:Dam rep.1
E
Frequency
Raw
Null
Raw - Null
log2 ratio (Ab:Dam/Dam)
F
Frequency
Raw
Null
Raw - Null
log2 ratio (Dam:Kn/Dam)

Figure S2 (Related to Figure 2). DamID data

(A) DamID profiles of Ab and Kn in the 415-618 kb region of chromosome 3L. Shown from the top are standardized log2-ratios of four biological replicates, averaged log2-ratios, smoothened log2-ratios, binding sites, and genes. (B-D) Pairwise plots of standardized log2-ratios at individual spots of Ab replicate 1 vs. Ab replicate 2 (B), Kn replicate 1 vs. Kn replicate 2 (C), Ab replicate 1 vs. Kn replicate 1 (D). Each correlation coefficient is indicated. (E and F) Binding sites were defined by subtracting null distributions (Null) from the raw distributions (Raw). Red lines indicate the modes; and blue lines, 3σ□of the null distribution (threshold values). See details such as red and blue lines in Analysis of DamID data in EXPERIMENTAL PROCEDURES.

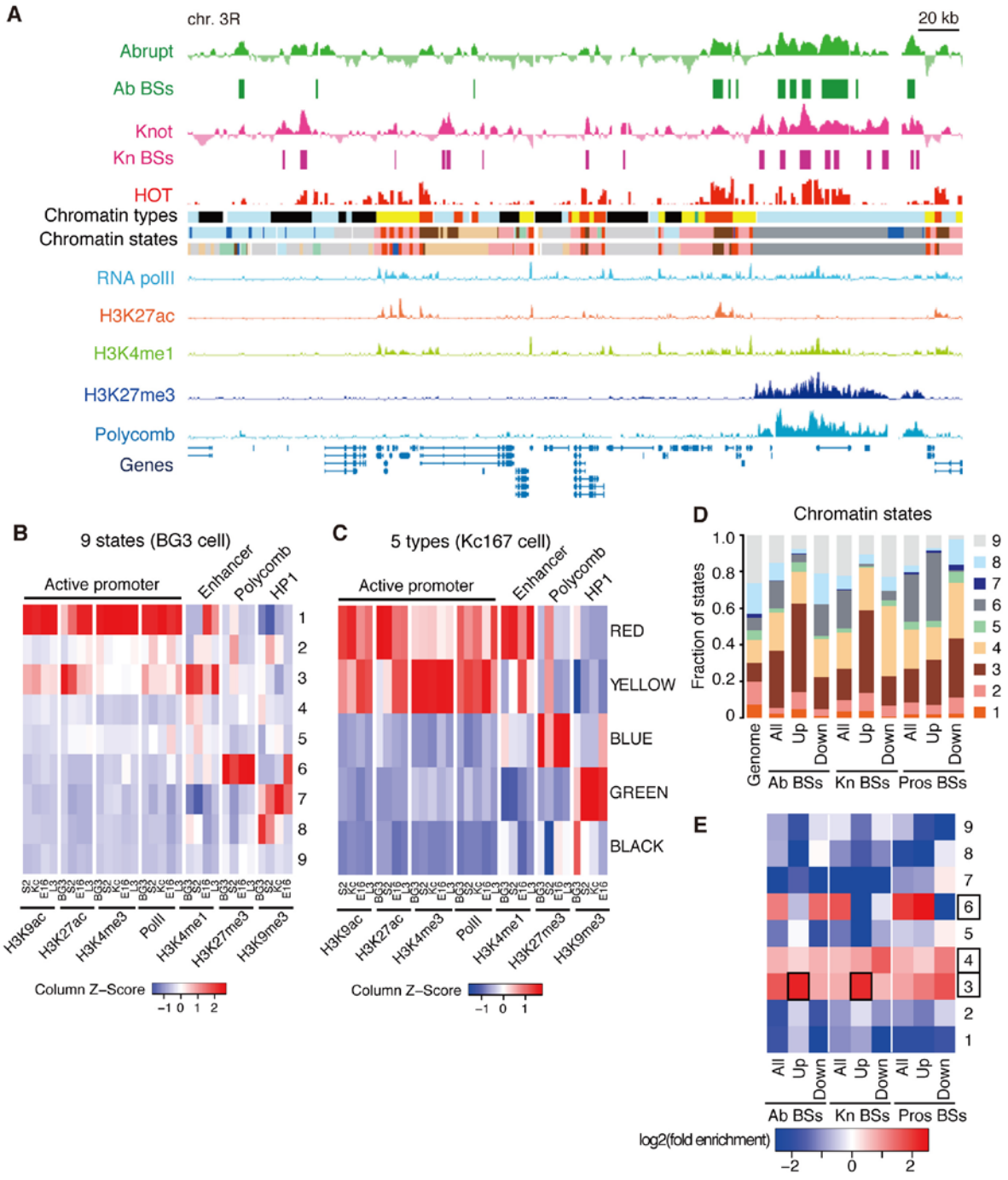

Figure S3 (Related to Figure 3). Enrichment of BSs of Ab or Kn in tissue-specific enhancers and Polycomb chromatin

(A) Examples of DamID profiles of Ab or Kn, distributions of Ab BSs, Kn BSs, and

HOT regions (Negre et al., 2011), chromatin types (Filion et al., 2010), chromatin states (Kharchenko et al., 2010) in BG3 cells (upper track) and those in S2 cells (lower track), and distributions of four chromatin marks (Negre et al., 2011) and Polycomb (Kwong et al., 2008) at embryonic stage. The 501-1002 kb region of chromosome 3R is shown.

(B and C) We confirmed that the combinatorial patterns of enrichments or paucities of the markers (such as those shown in “A”) are basically conserved among the cell lines, embryos that we used for DamID, and third-instar larvae from which we isolated da neurons for the expression profiling. Nine chromatin states were defined on the basis of data sets of the BG3 cell line, whereas five chromatin types were defined on the basis of those of the Kc167 cell line. Markers for chromatin features are indicated at the bottom. E16: embryonic stage (16–20 h AEL); L3: 3rd instar larval stage. For each sample (each column), enrichments or depletions of the markers in individual chromatin states (B) and types (C) are analyzed essentially as in Figure 3D and 3E, and color-coded by Z-score. The data sets are from the modENCODE consortium (Negre et al., 2011). The combinatorial patterns of the markers, such as H3K4me3 for active promoters, are conserved among the cell lines, E16, and L3.

(D and E) BSs of Ab, Kn, or Pros were sorted into chromatin states, and each fraction is shown (D). Enrichments/depletions of fractions of individual chromatin states are calculated relative to those in the genome and color-coded by fold enrichment (E). See details in the legends of Figure 3D and 3E. Prominent

selectivity was manifested by the large fractions of UP of the Ab and Kn BSs in state 3 chromatin that is classified into enhancers and intronic regulatory elements (Kharchenko et al., 2010) (red boxes with black frames), being consistent with the enrichment of the DamID BSs in introns (data not shown).

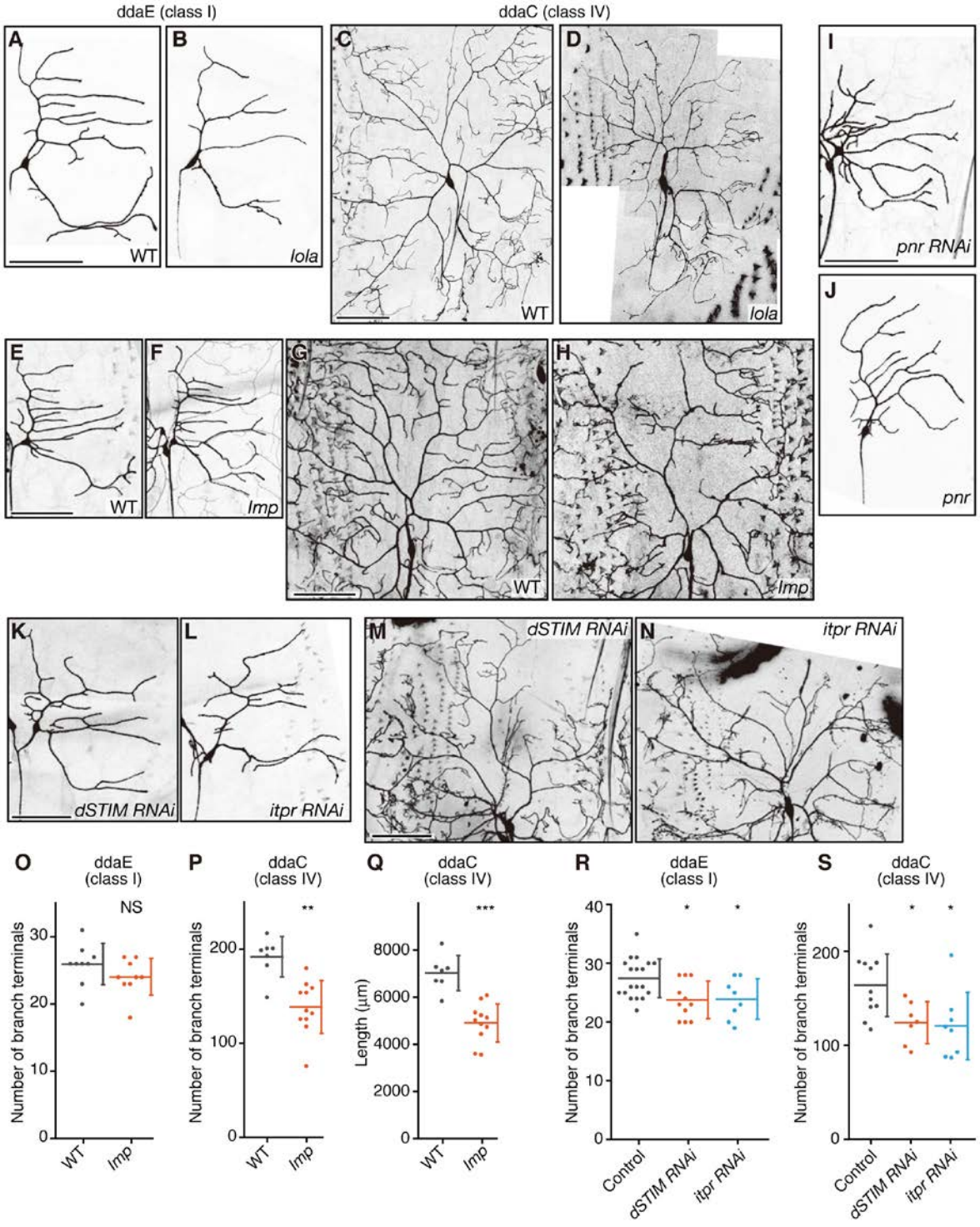

Figure S4 (Related to Figure 4) Phenotypes of mutant clones, da neurons in mutants, or knockdowns

(A-D) MARCM analysis. (A and C) Control clones of class I ddaE and class IV ddaC, respectively. (B and D) *lola* clones. Relevant clone genotypes are *hs-FLP, elav-Gal4 UAS-mCD8:GFP/SOP-FLP$^{\#42}$; FRT42D* (A and C) and *hs-FLP, elav-Gal4 UAS-mCD8:GFP/SOP-FLP$^{\#42}$; FRT42D lola^{C46}* (B and D).

(E-H, O-Q) ddaE and ddaC in the wild type (E and G, respectively) and in the *Imp^{8}* mutant (F and H, respectively). (O-Q) Quantitative analyses. The terminal number of the ddaE arbor (O). The terminal number (P), cumulative branch length (Q) of the dorsal sideof the ddaC arbor. Relevant genotypes are *+/Y; +; +/GAL4$^{2-21}$ UAS-mCD8:GFP* (E), *Imp^{8} /Y; +; +/GAL4$^{2-21}$ UAS-mCD8:GFP* (F), *+/Y; +; +/ppk-GAL4 UAS-mCD8:GFP* (G), *Imp^{8} /Y; +; +/ ppk-GAL4 UAS-mCD8:GFP* (H).

(I) Representative *pnr*-knockdown ddaE (*UAS-dicer2/UAS-pnr-RNAi (VDRC 101522); GAL4$^{2-21}$ UAS-mCD8:GFP/+*). (J) *pnr* mutant clone (*hs-FLP UAS-mCD8:GFP/+;Gal4$^{109(2)80}$ UAS-mCD8:GFP SOP-FLP$^{\#73}$/+; FRT82B pnr^{VX6}*).

(K-N, R, and S) *dSTIM*-knockdown ddaE and ddaC (K and M, respectively) and *itpr*-knockdown ddaE and ddaC (L and N, respectively). (R and S) Quantitative analyses of terminal numbers as described in O and P. Relevant genotypes are *UAS-dicer2/+; GAL4$^{2-21}$ UAS-mCD8:GFP/UAS-dSTIM-RNAi (TRiP27263)* (K), *UAS-dicer2/+; GAL4$^{2-21}$ UAS-mCD8:GFP/UAS-itpr-RNAi (VDRC 6484)* (L), *ppk-GAL4 UAS-mCD8:GFP/+; UAS-dicer2/ UAS-dSTIM-RNAi (TRiP27263)* (M), and *ppk-GAL4 UAS-mCD8:GFP/+; UAS-dicer2/UAS-itpr-RNAi (VDRC 6484)* (N). * $P < 0.05$, ** $P < 0.01$, *** $P < 0.001$. (O, P, and Q) Wilcoxon-Mann-Whitney test. (R and S) One-way ANOVA and HSD *post-hoc* test.

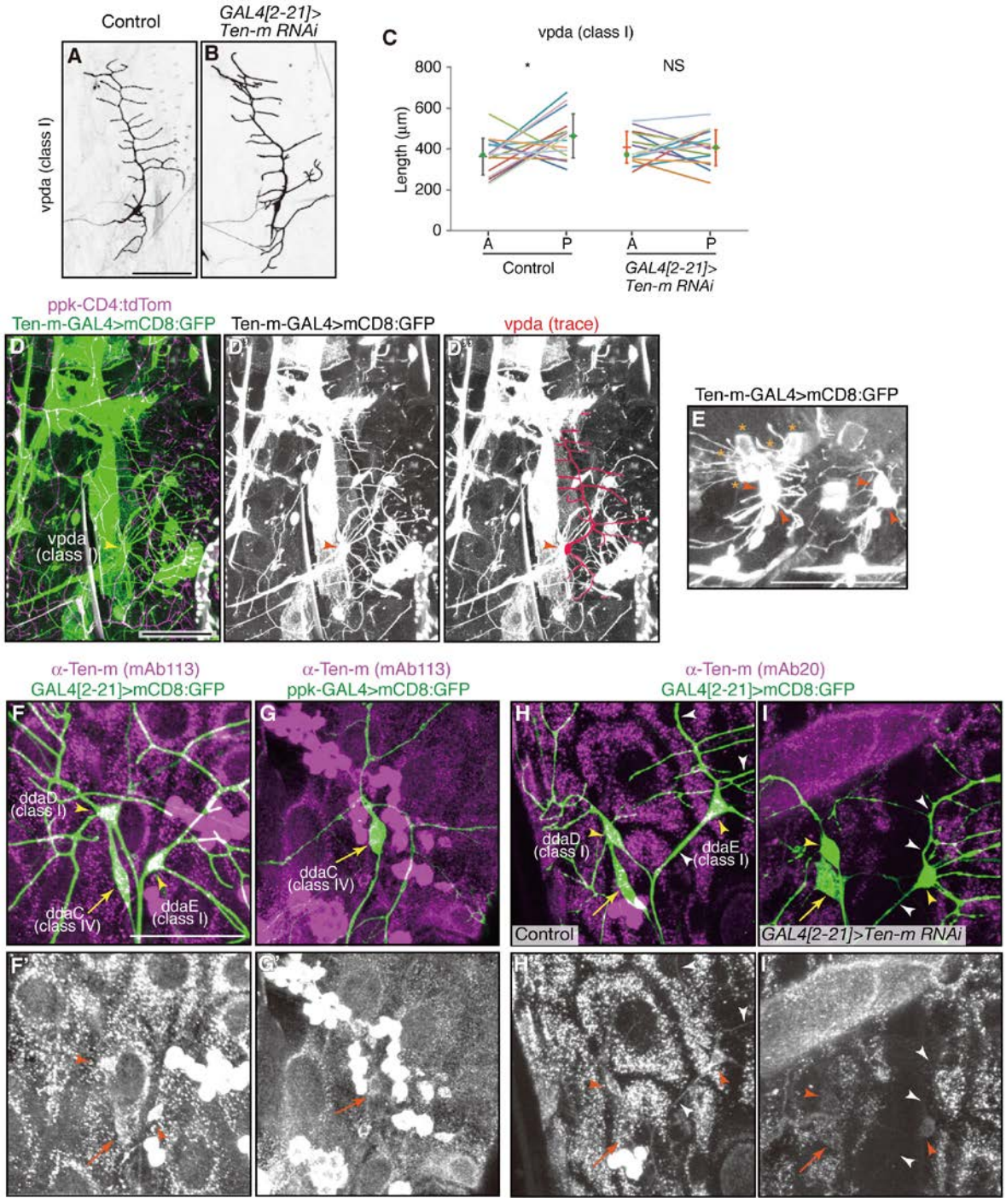

Figure S5 (Related to Figure 6) *Ten-m* knockdown phenotypes of class I vpda and *Ten-m* expression pattern

(A-C) (A) Control class I neuron vpda. (B) vpda when *Ten-m* was knocked down by using *GAL4[2-21]*. (C) Quantitative analysis. Length of individual branches anterior (A) to or posterior (P) to dorsally-oriented primary ones was measured and then the total length of A or P branches was plotted. Line segments identify the values from individual neurons. Median values are marked by green points. Error bars indicate the mean (horizontal bar) ± s.d. * $P < 0.05$ (Wilcoxon matched pairs test). The P-directed growth preference was lost by the knockdown (NS). When the ratio of the number of anterior-directed secondary branches to the number of posterior-directed secondary branches was compared (as we did for ddaE in Figure 6M), the difference was not statistically significant (data not shown).
(D-I') The *Ten-m* expression in a ventral region (D-D") and in dorsal regions (E-I') in larval hemisegments. Cell bodies of class I and IV neurons are marked by yellow or orange arrowheads and arrows, respectively. (D-D") *Ten-m* expression pattern was monitored by mCD8:GFP expression under the *Ten-m-GAL4* line. Dendritic branches of class I vpda are traced in D". (E) 24-27 hr AEL larva. Labeled cells include ddaD, ddaE (arrows), and a subset of epidermal cells (asterisks). (F-I') Representative images of antibody staining of Ten-m (magenta in F, G, H, and I; and F', G', H', and I') and the marker GFP (green in F, G, H, and I). In contrast to signals of Ten-m in class I neurons, only weak signals in class IV were observed. (H-I') Knockdown of *Tem-m* was confirmed by the reduced immunohistochemical signals in class I ddaD and ddaE. Control (Hand H') and *Tem-m-RNAi* (I and I'). Note that we sometimes detected Ten-m signals along dendrites or axons of class I

neuron ddaE (white arrowheads in H'). Relevant genotypes are *UAS-dicer2/+; GAL4*$^{2\text{-}21}$ *UAS-mCD8:GFP/+* (A, H, and H') and *UAS-dicer2/+; GAL4*$^{2\text{-}21}$ *UAS-mCD8:GFP/UAS-Ten-m-RNAi (VDRC51173)* (B, I and I'), +/*UAS-mCD8:GFP; NP6658/ppk-CD4:tdTom* (D-D''), +/*UAS-mCD8:GFP; NP6658/+* (E), *GAL4*$^{2\text{-}21}$ *UAS-mCD8:GFP/+* (F and F'), and *ppk-GAL4 UAS-mCD8:GFP/+* (G and G'). Bars, 100 µm (A and B, and D-D"); 50 µm (E and F-I').

Table S1 (Related to Figure 2). Lists of the Ab or Kn BSs, of the Ab- or Kn-bound, dependent or target genes, and genes that are regulated by Ab and Kn in quantitatively differential fashions

(see accompanying Excel spreadsheet)

Among candidates of target genes that have been reported previously (Crozatier and Vincent, 2008; Hattori et al., 2007; Jinushi-Nakao et al., 2007), *pickpocket* (*ppk*) was identified as one of *ab*-dependent genes in this study (1C and 1D; see also Table S3A).

Gene symbol	log2(fold change)			
	ab ME		*kn* ME	
	microarray	qPCR	microarray	qPCR
spin	1.3	3.7		NA
ssp4	0.9	3.3		NA
CG14642	2.2	NA	1.6	0.7
CG2201	1.5	NA	1.5	NA
lola	1.8	1.9	1.6	0.2
dOrai	1.7	*	1.6	*
CG31431	4.5	1.3	3.4	1.1
Ten-m	1.9	3.5	1.3	1.5
Imp	1.2	*	1.3	*
Pak3	1.5	2.9	1.5	1.1
tai	1.2	2.8	1.4	1.2
pnr	3.0	1.1	2.4	1.1
CG30080	-2.9	*		NA
Dab	-2.0	NA	-1.9	NA
hts	-1.4	-2.1		NA
ara	-1.0	NA		NA
BicD	-1.7	NA		NA
CG34347	-2.6	NA		NA
sdk	-1.5	NA		NA
CG31140	-3.5	NA	-2.4	*
dlp	-2.4	*	-2.2	*
SK	-2.7	*	-2.5	*
sog	-3.0	*	-1.4	*
Ptp10D	-2.2	-3.3	-1.6	-9.8

Table S2 (Related to Figure 2). Fold changes of expression levels of the

selected target genes

Comparison of log2(fold-change) made by triplicate microarray experiments and qPCR results for target genes listed in Table S4. An asterisk indicates that fold-change could not be calculated because cDNA from the control sample was not amplified. NA: not analyzed.

Table S3 (Related to Figure 2). List of the dependent and the bound genes implicated in neuronal differentiation or neuronal functions, or those encoding miRNA

(see accompanying Excel spreadsheet)

Target genes that yielded strong phenotypes of either class I and/or IV when knocked down

	Gene symbol	Gene function	Binding		Expression		Regulation	RNAi (Fig. 4)		OE (Fig. 5)		*kn* ME + RNAi (Fig. 5)
					ab ME	*kn* ME		I	IV	I	IV	
Up-regulated targets	***spin***	Endosome to lysosome transport	Ab		↑			M			R	NA
	***ssp4* (*Patronin*)**	Microtubule severing	Ab		↑			M	R, A	NA	NA	NA
	CG14642	Serine-type endopeptidase activity		Kn	↑	↑			P	NA	NA	+
	CG2201	Choline kinase activity		Kn	↑	↑		M		NA	NA	NA
	lola	Regulation of transcription	Ab	Kn	↑	↑	Ab↑↑ Kn↑	R	R	R	R	+
	***dOrai* (*olf186-F*)**	Store-operated Ca2+ release-activated Ca2+ channel	Ab	Kn	↑	↑		R	R		A	+
	CG31431	fibroblast growth factor-activated receptor activity	Ab	Kn	↑	↑		M	R	NA	NA	NA
	Ten-m	Cell adhesion	Ab	Kn	↑	↑	Ab↑↑ Kn↑	M	A		M	-
	Imp	mRNA binding	Ab	Kn	↑	↑			R		I	+
	Pak3	Receptor signaling protein serine/threonine kinase activity	Ab	Kn	↑	↑			R	M	A	+
	tai	Transcription coactivator activity	Ab	Kn	↑	↑		R		R, M	A	NA
	pnr	Regulation of transcription	Ab	Kn	↑	↑		M		NA	NA	NA
Down-regulated targets	***CG30080***	Regulation of transcription	Ab		↓			M		NA	NA	NA
	Dab	Signaling pathway	Ab		↓	↓		M			A	NA
	hts	Actin capping	Ab	Kn	↓			M	A	NA	NA	NA
	ara	Regulation of transcription	Ab	Kn	↓			M			R	NA
	BicD	RNA transport	Ab	Kn	↓			M				NA
	CG34347	Actin binding	Ab	Kn	↓			M		NA	NA	NA
	sdk	Pigment cell differentiation	Ab	Kn	↓			M		NA	NA	NA
	CG31140	Diacylglycerol kinase activity		Kn	↓	↓		M		NA	NA	NA
	dlp	Glypican-type heparan sulfate proteoglycan	Ab	Kn	↓	↓		M	M, A		A	NA
	SK	Small conductance calcium-activated potassium channel	Ab	Kn	↓	↓		M		NA	NA	NA
	sog	BMP signaling pathway	Ab	Kn	↓	↓	Ab↓↓ Kn↓	M		NA	NA	NA
	Ptp10D	Protein amino acid dephosphorylation	Ab	Kn	↓	↓			R	NA	NA	NA

A: Abnormal terminals, I: Increased arborization, M: Misrouting, P: Positioning of branch points, R: Reduced arborization

Table S4 (Related to Figure 4 and 5). Target genes that yielded strong

phenotypes of either class I and/or IV when knocked down

The column labeled “Binding” indicates whether each target gene was bound by Ab, Kn, or both, and colored letters indicate altered expression by Ab and/or Kn. In the column of “Expression”, upward and downward arrows indicate up-regulation and down-regulation by Ab or Kn misexpression (ME), respectively. The column labeled “Regulation” indicates target genes that were either up- or down-regulated more strongly by Ab ME. In the columns labeled “RNAi” and “OE”, only knockdown or overexpression that gave strong phenotypes in “I” (class I) or “IV” (class IV) are labeled. We have categorized those phenotypes and have added annotations at the bottom. NA: not analyzed. In the columns labeled “*kn* ME + RNAi”, knockdowns that suppressed *kn* ME phenotype are labeled as “+”.

SUPPLEMENTAL EXPERIMENTAL PROCEDURES

Drosophila strains

We used *GAL4*$^{21\text{-}7}$ *UAS-mCD8:GFP* (Song et al., 2007), *UAS-abL* and *UAS-abS* (Sugimura et al., 2004), *UAS-Kn:HA* (Hattori et al., 2007), *GAL4*$^{2\text{-}21}$ *UAS-mCD8:GFP* (Grueber et al., 2003), *ppk-GAL4 UAS-mCD8:GFP* on the 2nd chromosome (Kimura et al., 2006) or on the 3rd chromosome (Grueber et al., 2007), *UAS-dicer2* and RNAi stocks (Vienna *Drosophila* RNAi Center), *UAS-spin-RFP* (gift from S. Sweeney and G. Davis), *UAS-Imp-SD* (Boylan et al., 2008) and *Imp*^{8} (Munro et al., 2006), *UAS-lolaL* (Spletter et al., 2007) and *FRT42D lola*^{C46} (Horiuchi et al., 2003), *NP6658*-GAL4 (*Ten-m-GAL4*; *Drosophila* Genomics Resource Center) *UAS-ten-m* (Mosca et al., 2012), *FRT82B pnr*^{VX6} and *arm-GAL4* (Bloomington Stock Center), *hh-GAL4* (Tanimoto et al., 2000), *ppk-CD4:tdGFP* and *ppk-CD4:tdTom* (Han et al., 2011) and sensory organ precursor (SOP)-FLP stocks (Matsubara et al., 2011). Fly embryos and larvae were grown at 29 °C for RNAi and overexpression experiments and at 25°C for other experiments.

DamID experiments

To express Dam fusion proteins, we first constructed pUAST-NDam and pUAST-CDam plasmids by cloning the Dam-Myc sequence from pNDamMyc and pCMycDam (van Steensel et al., 2001), respectively, into the multiple cloning site of pUAST (Brand and Perrimon, 1993). Full-length coding sequences from *ab* and *kn*

were amplified from cDNA clones RE25924 and RE03728, respectively, and cloned into pUASTNDam or pUASTCDam. *UAS* transgenic lines were generated and a reference stock *UAS-Dam* has been described previously (Choksi et al., 2006). These Dam fusion proteins were expressed in eye discs using *GMR-GAL4* (Bloomington 8605). On the basis of their subcellular localization and expression levels in comparison to those of Dam, *UAS-Abrupt:Dam* and *UAS-Dam:Knot* lines were selected for the following experiments.

We expressed the Dam fusion proteins in da neurons and examined dendrite phenotypes. Forced expression of Ab:Dam in classes II-IV neurons downsized and simplified their dendritic arbors, transforming them into class I-like, phenocopying misexpression of Ab (Sugimura et al., 2004); likewise, Dam:Kn expression in classes other than IV increased the complexity of their dendritic arbors, as Kn misexpression does (Hattori et al., 2007) (data not shown). These results supported the assumption that each fusion protein bound to regulatory sequences of the presumptive target genes that we looked for.

For DamID, stage 17 embryos (17–20 h AEL) of the following genotypes were collected: *yw*; *UAS-Dam*/+, *yw*; *UAS-Abrupt:Dam*/+, or *yw*; *UAS-Dam:Knot*/+. To express the Dam or the Dam fusion proteins at a leaky level, *GAL4* drivers were deliberately omitted from the expression protocol. DNA isolation, processing, and amplification were performed as described previously (Choksi et al., 2006). The DNA samples were labeled with Cy3 or Cy5 and hybridized to a custom whole-genome tiling array with 60-mer oligonucleotides spaced at ~300 bp intervals (Choksi et al.,

2006), and four biological replicates were performed. Arrays were scanned and intensities were extracted (NimbleGen Systems). Log2 mean signal ratios of TF-Dam/Dam at individual spots were median scaled, and four binding profiles for each of Ab:Dam or Dam:Kn were obtained.

Analysis of DamID data.

Scaled log2 ratios were preprocessed as previously described (Kind et al., 2008; Schwartz et al., 2006). The following formula was used to standardize variances of scaled log2 ratios of each replicate:

$Z = (X - \mu)/\sigma$

(X: scaled log2-ratio, μ: mean of scaled log2-ratio, σ: standard deviation of scaled log2-ratio).

The standardized log2-ratios of the four replicates ("Ab rep.1-rep.4 and Kn rep.1-rep.4" in Figure S2A) were averaged and smoothed by using a 1400 bp window centered on each probe to correct for variability in probe annealing properties ("smoothed" in Figure S2A). Within the Ab or Kn replicates, every profile was highly correlated with the other (Figure S2B-S2C); in contrast, this was not the case between the different TF replicates (Figure S2D).

Binding sites (BSs) were defined as follows: the distributions of the smoothed ratios were skewed towards positive values (raw distributions or "Raw" in Figure S2E and S2F). All statistics falling below the mode (red lines in Figure S2E and S2F) were used to estimate the left side of the null distribution (Schwartz et al., 2006);

then the full null distribution was obtained by reflecting the left side of the null distribution onto the right side of the mode (van Steensel et al., 2003). The null distribution was subtracted from the raw distribution ("Raw – Null" in Figure S2E and S2F) and threshold values were set as 3σ□of the null distribution (blue lines in Figure S2E and S2F). The regions with signal ratios above the thresholds were defined as BSs. Consequently, only 0.15% of estimated noise was included in the BSs. Bound genes were defined as follows: genes containing BSs were chosen; if a BS was located between two genes, we chose both. The tool for presenting the binding profile and viewing genomic data sets was the University of California-Santa Cruz (UCSC) Genome Browser (Fujita et al., 2011) (e.g., Figure 2A).

The number of bound genes of the following TFs are: 1,214 (Prospero), 1,082 (Asense), 1,243 (Snail), and 696 (Deadpan), as reported previously by DamID studies using Drosophila embryos (Choksi et al., 2006; Southall and Brand, 2009), although it should be noted that BSs and bound genes are defined somewhat differently from this study. In (Southall and Brand, 2009) and (Negre et al., 2011), bound genes are defined when a binding event occurs within 5kb (Asense, Snail, and Deadpan) or up to 1kb (Prospero) of the gene structure. On the other hand, we did not set a limit on the distance of the gene from the BS. This was because previous studies on cis-regulatory elements show that the distance from BSs of TFs to their target genes is quite variable (Haeussler and Joly, 2011). Our Dam:Knot Dam ID experiment was validated at least by detecting BSs 1.7 kb upstream of *kn* itself, which are used for auto-regulation in muscles (Dubois et al., 2007). BSs identified by

DamID have been shown to match those identified by chromatin immunoprecipitation (Song et al., 2004; Sun et al., 2003; Tolhuis et al., 2006) and by 3D microscopy data (Guelen et al., 2008; Pickersgill et al., 2006). We conducted de novo motif analysis of Ab and Kn BSs by using MEME-ChIP (Machanick and Bailey, 2011), Cistrome SeqPos/CEAS (Shin et al., 2009) and rGADEM (Li, 2009), but did not obtain consistent results between these algorithms (data not shown).

Custom Perl scripts, R package (http://www.R-project.org), and the Bioconductor package were used for data analysis in general including calculations of fold enrichments essentially as described previously (Negre et al., 2011). For making heat maps, heatmap.2 in the gplots package of R was used. The Kn BSs in this study and those from the modENCODE data were not tightly clustered (Figure 3A), possibly due to a difference of developmental stage, and such examples are seen in a previous report (Negre et al., 2011).

Expression profiling of isolated da neurons

da neurons were isolated from larvae of three distinct genotypes: *+/GAL4$^{21\text{-}7}$ UAS-mCD8:GFP* (control), *+/GAL4$^{21\text{-}7}$ UAS-mCD8:GFP; UAS-abL/+* (*ab* ME), and *UAS-knL:HA/GAL4$^{21\text{-}7}$ UAS-mCD8:GFP* (*kn* ME). *GAL4$^{21\text{-}7}$*drives gene expression exclusively in multidendritic sensory neurons, including all da classes (Song et al., 2007), but its expression was not strong enough in embryos. Consequently, we isolated da neurons using magnetic beads from larvae and prepared RNA basically as described (Iyer et al., 2009), with the following modifications: 1) We

dissected wandering third instar larvae, inverted their body walls in ice-cold dissecting saline, and immediately transferred them into SM[active] medium on ice (Nagoshi et al., 2010). 2) Biotin-conjugated anti-mouse CD8a antibody (Ly-2 of eBioscience) and a 1 ml dounce tissue grinder (Wheaton) were used. 3) Cell solutions were triturated by using a flame-rounded Pasteur pipette followed by a flame-rounded 200-μl pipetter tip with filter, until most of the tissues were dissociated to single cells. RNA was purified from 80 larvae of each genotype, making three sets of RNA samples.

The RNA samples were amplified with a WT-Ovation Pico RNA Amplification System (NuGEN), labeled, hybridized to Affymetrix Drosophila Genome 2.0 Arrays by Takara Bio Inc., and data of triplicates were obtained. Raw Affymetrix .CEL files were preprocessed using RMA (Irizarry et al., 2003). The data was analyzed using the Bioconductor limma package (Smyth, 2004) with the arrayWeights function to detect differential gene expression. Statistical significance of the results was determined using a moderated eBayes t-test. The resulting P-values were adjusted using FDR (Benjamini and Hochberg, 1995). Probe sets were mapped to genes using the annotation available in FlyBase (r5.35). We defined instances with the adjusted P-values < 0.05 as significant changes. We found that the *ppk* level was down-regulated (the log2(fold change) was -2.31) by *ab* ME as expected from previous studies (Hattori et al., 2007).

We examined the increase or the decrease in the expression levels of a subset of target genes by qPCR and/or immunohistochemistry (see also “Imaging

dendritic trees, immunohistochemistry, in situ hybridization, quantification and statistical tests" below). For qPCR, ReverTra Ace and Thunderbird (TOYOBO) were used according to the manufacturers' instructions. Out of the twenty genes, using *gapdh* or *rp49* as a reference, the cDNA levels of fourteen (*Ten-m*, *lola*, *pak3*, *tai*, *Ptp10D*, *spin*, *ssp4*, *hts*, *CG14642 CG31140*, *CG31431*, *Gap1*, *pnr*, and *RhoGAP19D*) were either increased or decreased as shown in the microarray data and the fold changes are indicated in Table S2. For the other six (*dOrai*/*Olf186-F*, *Imp*, *dlp*, *SK*, *sog*, and *CG30080*), cDNA was not amplified from the control sample, thus fold-change could not be calculated.

Although we planned expression profiling of *ab* or *kn* loss-of-function conditions, the *ab* mutant was early larval lethal and only a small fraction of *kn* homozygous mutant embryos survived to late embryonic stages, making collection of enough numbers of da neurons from the mutant larvae prohibitively difficult. We also attempted to knock down *ab* or *kn* by using drivers such as *GAL4*$^{2\text{-}21}$ for class I or *ppk-Gal4* for class IV; however, cellular phenotypes were much less dramatic than those of *ab* or *kn* mutant clones possibly due to late onset of *GAL4* expression. Nonetheless, we argue that target genes we identified in this study include those that are indeed transcriptionally regulated by Ab or Kn and contribute to dendrite morphogenesis under the control of Ab or Kn. Our supporting evidence is the following:

1. We confirmed that expression of *lola*, which is one of the up-regulated common targets, was decreased in *ab* or *kn* mutant embryos, whereas it was

increased in *ab* or *kn* ME/overexpression larvae (Figure S1).

2. *ab* ME or *kn* ME severely affected morphologies of dendritic arbors (Figure 1E-1G'), presumably due to altered expression levels of target genes.
3. Out of the six up-regulated targets which we showed were required for class IV arbor formation, knockdowns of five of them significantly suppressed the *kn* ME class IV-like transformation phenotype of class I neurons (Figure 5G, 5H and 5J; Table S4), supporting the idea that up-regulation of the Kn target genes that we identified contributed to the class IV-like transformation of class I neurons.

RNAi

Using the list of the target genes, we conducted a small-scale in situ hybridization screening and found that probes for genes with no GO annotation gave signals in embryos barely above the limit of sensitivity of our experimental conditions (data not shown). Thus, we selected 103 genes on the basis of GO terms and performed a primary RNAi screening. 32 genes exhibited morphological defects in dendritic arbors of class I and/or IV when knocked down. Out of these 32, we conducted a secondary RNAi screening using available transgenic stocks of dsRNA targeted to other sequences; and we also examined the effects of overexpression of 11 genes whose UAS strains have been published. The *GAL4* drivers employed were *GAL4*$^{2\text{-}21}$ *UAS-mCD8:GFP* for class I and *ppk-Gal4 UAS-mCD8:GFP* on the 2nd chromosome for class IV. The RNAi efficacy of *lola* or *Ten-m* was assessed and

verified by the reduction of antibody staining (Figure S1E and S5H-S5I'). In knocking down or overexpressing each gene, 6-15 pairs of the class I neurons (ddaD and ddaE) and 3-15 class IV ddaC were observed, phenotypes were searched visually, and then quantitatively analyzed (Figures 4-5).

To examine the effects of knockdowns of *ab* target genes on *ab* misexpression-induced transformation of the class IV dendritic arbor, we attempted to co-express *ab* and dsRNA of Ab target genes in class IV (for a purpose analogous to that of Figure 5E-5H). However, none of the class IV-selective *GAL4* drivers tested worked together with *ab* misexpression (we previously showed the effect of ab misexpression on class IV by using a pan-da driver and subsequent ablation of class I-III; see Sugimura et al., 2004). Those were *ppk-Gal4*, *stj-GAL4(Ly et al., 2008)*, *GAL4*$^{4\text{-}77}$ (Emoto et al., 2004), and *Gr28b.c-GAL4* (Xiang et al., 2010). This was most likely because ectopic expression of *ab* shuts down promoters where *GAL4*-containig vectors are inserted (Hattori et al., 2007).

To knock down *Ten-m* in adjacent tissues such as epidermis, we examined expression patterns in several GAL4 drivers previously described (Parrish et al., 2009). We found that (1) *arm-GAL4* expression was high in epidermis and a subset of muscles, (2) *69B-GAL4* expression in epidermis was variable from one hemi-segment to another and sometimes it was absent in epidermis overlaying da neurons of the dorsal cluster (that was why we did not use *69B-GAL4* in this study), and (3) very low-level expression of *arm-GAL4* was detected in some ddaC-ddaE and that of *69B*-GAL4 was in ddaC, whereas *hh-GAL4* expression was detected in

none of the da neurons (data not shown).

Genotypes

Exact genotypes of individual animals used in Figures 1-8 are as follows unless described in the legends:

Figure 1

(A) *Gal4$^{2\text{-}21}$ UAS-mCD8:GFP/+*

(B) *Gal4$^{5\text{-}40}$ UAS-Venus-pm, SOP-FLP$^{\#42}$/+; FRT40A/ FRT40A tubP-Gal80*

(E and E') *+/GAL4$^{21\text{-}7}$ UAS-mCD8:GFP*

(F and F') *+/ GAL4$^{21\text{-}7}$ UAS-mCD8:GFP; UAS-abL/+*

(G and G') *UAS-knL:HA/GAL4$^{21\text{-}7}$ UAS-mCD8:GFP*

Figure 4

(A) *UAS-dicer2/+; GAL4$^{2\text{-}21}$ UAS-mCD8:GFP/+*

(B) *UAS-dicer2/+; GAL4$^{2\text{-}21}$ UAS-mCD8:GFP/UAS-spin-RNAi(TRiP27702)*

(C) *UAS-dicer2/+; GAL4$^{2\text{-}21}$ UAS-mCD8:GFP/UAS-dOrai-RNAi(VDRC12221)*

(D) *UAS-dicer2/+; GAL4$^{2\text{-}21}$ UAS-mCD8:GFP/UAS-lola-RNAi(VDRC101925)*

(E) *UAS-dicer2/+; GAL4$^{2\text{-}21}$ UAS-mCD8:GFP/UAS-Imp-RNAi(VDRC20321)*

(F) *ppk-GAL4 UAS-mCD8:GFP/+; UAS-dicer2/+*

(G) *ppk-GAL4 UAS-mCD8:GFP/+; UAS-dicer2/UAS-CG14642-RNAi (VDRC14047)*

(H) *ppk-GAL4 UAS-mCD8:GFP/+; UAS-dicer2/UAS-dOrai-RNAi(VDRC12221)*

(I) *ppk-GAL4 UAS-mCD8:GFP/+; UAS-dicer2/UAS-lola-RNAi(VDRC101925)*

(J) *ppk-GAL4 UAS-mCD8:GFP/+; UAS-dicer2/UAS-Imp-RNAi(VDRC20321)*

Figure 5

(A) *ppk-GAL4 UAS-mCD8:GFP/+*

(B) *ppk-GAL4 UAS-mCD8:GFP/UAS-spin-RFP*

(C) *ppk-GAL4 UAS-mCD8:GFP/UAS-Imp-SD*

(D) *ppk-GAL4 UAS-mCD8:GFP/UAS-lolaL*

(E) *UAS-dicer2/+; GAL4$^{2-21}$ UAS-mCD8:GFP/+*

(F) *UAS-dicer2/UAS-Kn:HA; GAL4$^{2-21}$ UAS-mCD8:GFP/+*

(G) *UAS-dicer2/UAS-Kn:HA; GAL4$^{2-21}$ UAS-mCD8:GFP/UAS-dOrai-RNAi (VDRC12221)*

(H) *UAS-dicer2/UAS-lola-RNAi (VDRC101925); GAL4$^{2-21}$ UAS-mCD8:GFP/UAS-Kn:HA*

Figure 6

(A) *UAS-dicer2/+; GAL4$^{2-21}$ UAS-mCD8:GFP/+*

(B) *UAS-dicer2/+; GAL4$^{2-21}$ UAS-mCD8:GFP/UAS-Ten-m-RNAi (VDRC51173)*

(C and C') *UAS-dicer2/arm-GAL4*

(D and D') *UAS-dicer2/+; +/arm-GAL4; UAS-Ten-m-RNAi (VDRC51173)/+*

(E, E', F, H, and H') *+/UAS-mCD8:GFP; NP6658/ppk-CD4:tdTom*

(I) *+/FRT40A; +/NP6658,UAS-mCD8:GFP*

(J) *ab^{clu1}/ab^{k02807} FRT40A* ; *+/NP6658,UAS-mCD8:GFP*

(K and K') *+/hh-GAL4 UAS-GFP*

(L and L') *UAS-Ten-m/hh-GAL4 UAS-GFP*

Figure 7

(A, G, G', and O) *ppk-GAL4 UAS-mCD8:GFP/+; UAS-dicer2/+*

(B, H, H', and P) *ppk-GAL4 UAS-mCD8:GFP/+; UAS-dicer2/UAS-Ten-m-RNAi (VDRC51173)*

(C, I, I', and Q) *UAS-dicer2/ppk-CD4:tdGFP; +/NP6658*

(D, J, J', and R) *UAS-dicer2/+; +/ppk-CD4:tdGFP; UAS-Ten-m-RNAi (VDRC51173)/NP6658*

(E, K, K', M, M', S, and U) *UAS-dicer2/ ppk-CD4:tdTom; +/hh-GAL4 UAS-GFP*

(F, L, L', N, N', T, and V) *UAS-dicer2/+; +/ ppk-CD4:tdTom; UAS-Ten-m-RNAi (VDRC51173)/hh-GAL4 UAS-GFP*

Figure 8

(A and A') *ppk-GAL4 UAS-mCD8:GFP/+*

(B and B') *ppk-GAL4 UAS-mCD8:GFP/UAS-Ten-m*

(C and C') *GAL4$^{2\text{-}21}$ UAS-mCD8:GFP/+*

(D and D') *GAL4$^{2\text{-}21}$ UAS-mCD8:GFP/UAS-Ten-m*

Immunohistochemistry and statistical tests

Other antibodies employed for immunohistochemistry were anti-Spin (Sweeney and Davis, 2002), anti-IMP (Adolph et al., 2009), anti-Pak3 (Bahri et al., 2010), and anti-Tai (Bai et al., 2000). In contrast to restricted nuclear localization of Lola, the other proteins were distributed in both cell bodies and dendritic branches, making quantitative comparisons between genotypes difficult. Actual P values are as follows:

Figure 4

(K) From left to right, 0.9456, < 0.0001, < 0.0001, and 0.8374

(L) 0.0111

(M) From left to right, 1, 0.0014, 0.4345, and 0.7542

(N) From left to right, 0.1827, < 0.0001, and 0.0001

(O) 0.0013

Figure 5

(I) From left to right, < 0.0001, 0.0004, and 0.0035

(Black in J) From left to right, < 0.0001, < 0.0001, 0.078, 0.0732, < 0.0001, < 0.0001, < 0.0001, and < 0.0001

(Blue in J) From left to right, < 0.0001, < 0.0001, < 0.0001, 0.0118, 0.0092, and 0.3349

Figure 6

(G) < 0.0001

(M) From left to right, 0.0055, 0.0021, 0.0001, 0.0037

(N) 0.0005

Figure 7

(O and P) 0.0058

(Q and R) < 0.0001

(S and T) < 0.0001

(U and V) 0.0502

Figure 8

(E) 0.0037 (Control class IV vs. *Ten-m OE* class IV), 0.0012 (Control class IV vs. Control class I), 0.0001 (Control class IV vs. *Ten-m OE* class I), 0.9965 (*Ten-m OE* class IV vs. Control class I), and 0.9071 (Control class I vs. *Ten-m OE* class I).

(F) 0.1885 (Control class IV vs. *Ten-m OE* class IV), < 0.0001 (Control class IV vs. Control class I), < 0.0001 (Control class IV vs. *Ten-m OE* class I), < 0.0001 (*Ten-m OE* class IV vs. Control class I), and 0.9998 (Control class I vs. *Ten-m OE* class I).

Figure S1

(D) < 0.0001 (Control vs. *ab* ME), 0.0071 (Control vs. *kn* ME), and < 0.0001 (*ab* ME vs. Kn ME)

(E) 0.0002

(F) 0.0007 (Control vs. *ab* ME), < .0001 (Control vs. *kn* ME), and 0.283 (*ab* ME vs. *kn* ME)

(G) 0.0002 (WT vs. ab^{k02807}/ab^{clu1}), 0.0005 (WT vs. kn^{KN2}/kn^{KN4}), and 0.9219 (ab^{k02807}/ab^{clu1} vs. kn^{KN2}/kn^{KN4}))

(H) < 0.0001 (WT vs. ab^{k02807}/ab^{clu1}), < 0.0001 (WT vs. kn^{KN2}/kn^{KN4}), and 0.9944 (ab^{k02807}/ab^{clu1} vs. kn^{KN2}/kn^{KN4})

Figure S4

(O) 0.2087

(P) 0.0028

(Q) 0.0003

(R) From left to right, 0.0154 and 0.0404

(S) From left to right, 0.0413 and 0.0194

Figure S5

(C) From left to right, 0.0250 and 0.8904

SUPPLEMENTAL REFERENCES

Bahri, S., Wang, S., Conder, R., Choy, J., Vlachos, S., Dong, K., Merino, C., Sigrist, S., Molnar, C., Yang, X.*, et al.* (2010). The leading edge during dorsal closure as a model for epithelial plasticity: Pak is required for recruitment of the Scribble complex and septate junction formation. Development *137*, 2023-2032.

Bai, J., Uehara, Y., and Montell, D.J. (2000). Regulation of invasive cell behavior by taiman, a Drosophila protein related to AIB1, a steroid receptor coactivator amplified in breast cancer. Cell *103*, 1047-1058.

Benjamini, Y., and Hochberg, Y. (1995). Controlling the False Discovery Rate - a Practical and Powerful Approach to Multiple Testing. J Roy Stat Soc B Met *57*, 289-300.

Brand, A.H., and Perrimon, N. (1993). Targeted gene expression as a means of altering cell fates and generating dominant phenotypes. Development *118*, 401-415.

Emoto, K., He, Y., Ye, B., Grueber, W.B., Adler, P.N., Jan, L.Y., and Jan, Y.N. (2004). Control of dendritic branching and tiling by the Tricornered-kinase/Furry signaling pathway in Drosophila sensory neurons. Cell *119*, 245-256.

Fujita, P.A., Rhead, B., Zweig, A.S., Hinrichs, A.S., Karolchik, D., Cline, M.S., Goldman, M., Barber, G.P., Clawson, H., Coelho, A.*, et al.* (2011). The UCSC Genome Browser database: update 2011. Nucleic acids research *39*, D876-882.

Grueber, W.B., Jan, L.Y., and Jan, Y.N. (2003). Different levels of the homeodomain protein cut regulate distinct dendrite branching patterns of Drosophila multidendritic neurons. Cell *112*, 805-818.

Grueber, W.B., Ye, B., Yang, C.H., Younger, S., Borden, K., Jan, L.Y., and Jan, Y.N. (2007). Projections of Drosophila multidendritic neurons in the central nervous system: links with peripheral dendrite morphology. Development *134*, 55-64.

Guelen, L., Pagie, L., Brasset, E., Meuleman, W., Faza, M.B., Talhout, W., Eussen, B.H., de Klein, A., Wessels, L., de Laat, W.*, et al.* (2008). Domain organization of human chromosomes revealed by mapping of nuclear lamina interactions. Nature *453*, 948-951.

Haeussler, M., and Joly, J.S. (2011). When needles look like hay: how to find tissue-specific enhancers in model organism genomes. Developmental biology *350*, 239-254.

Han, C., Jan, L.Y., and Jan, Y.N. (2011). Enhancer-driven membrane markers for analysis of nonautonomous mechanisms reveal neuron-glia interactions in Drosophila. Proceedings of the National Academy of Sciences of the United States of America *108*, 9673-9678.

Horiuchi, T., Giniger, E., and Aigaki, T. (2003). Alternative trans-splicing of constant and variable exons of a Drosophila axon guidance gene, lola. Genes & development *17*, 2496-2501.

Irizarry, R.A., Bolstad, B.M., Collin, F., Cope, L.M., Hobbs, B., and Speed, T.P. (2003). Summaries of Affymetrix GeneChip probe level data. Nucleic acids research *31*, e15.

Kimura, H., Usui, T., Tsubouchi, A., and Uemura, T. (2006). Potential dual molecular interaction of the Drosophila 7-pass transmembrane cadherin Flamingo in dendritic morphogenesis. Journal of cell science *119*, 1118-1129.

Kind, J., Vaquerizas, J.M., Gebhardt, P., Gentzel, M., Luscombe, N.M., Bertone, P., and Akhtar, A. (2008). Genome-wide analysis reveals MOF as a key regulator of dosage compensation and gene expression in Drosophila. Cell *133*, 813-828.

Kwong, C., Adryan, B., Bell, I., Meadows, L., Russell, S., Manak, J.R., and White, R. (2008). Stability and dynamics of polycomb target sites in Drosophila development. PLoS genetics *4*, e1000178.

Li, L. (2009). GADEM: a genetic algorithm guided formation of spaced dyads coupled with an EM algorithm for motif discovery. Journal of computational biology : a journal of computational molecular cell biology *16*, 317-329.

Ly, C.V., Yao, C.K., Verstreken, P., Ohyama, T., and Bellen, H.J. (2008). straightjacket is required for the synaptic stabilization of cacophony, a voltage-gated calcium channel alpha1 subunit. The Journal of cell biology *181*, 157-170.

Machanick, P., and Bailey, T.L. (2011). MEME-ChIP: motif analysis of large DNA datasets. Bioinformatics *27*, 1696-1697.

Munro, T.P., Kwon, S., Schnapp, B.J., and St Johnston, D. (2006). A repeated IMP-binding motif controls oskar mRNA translation and anchoring independently of Drosophila melanogaster IMP. The Journal of cell biology *172*, 577-588.

Nagoshi, E., Sugino, K., Kula, E., Okazaki, E., Tachibana, T., Nelson, S., and Rosbash, M. (2010). Dissecting differential gene expression within the circadian neuronal circuit of Drosophila. Nature neuroscience *13*, 60-68.

Pickersgill, H., Kalverda, B., de Wit, E., Talhout, W., Fornerod, M., and van Steensel,

B. (2006). Characterization of the Drosophila melanogaster genome at the nuclear lamina. Nature genetics *38*, 1005-1014.

Schwartz, Y.B., Kahn, T.G., Nix, D.A., Li, X.Y., Bourgon, R., Biggin, M., and Pirrotta, V. (2006). Genome-wide analysis of Polycomb targets in Drosophila melanogaster. Nature genetics *38*, 700-705.

Shin, H., Liu, T., Manrai, A.K., and Liu, X.S. (2009). CEAS: cis-regulatory element annotation system. Bioinformatics *25*, 2605-2606.

Smyth, G.K. (2004). Linear models and empirical bayes methods for assessing differential expression in microarray experiments. Statistical applications in genetics and molecular biology *3*, Article3.

Song, S., Cooperman, J., Letting, D.L., Blobel, G.A., and Choi, J.K. (2004). Identification of cyclin D3 as a direct target of E2A using DamID. Molecular and cellular biology *24*, 8790-8802.

Song, W., Onishi, M., Jan, L.Y., and Jan, Y.N. (2007). Peripheral multidendritic sensory neurons are necessary for rhythmic locomotion behavior in Drosophila larvae. Proceedings of the National Academy of Sciences of the United States of America *104*, 5199-5204.

Sun, L.V., Chen, L., Greil, F., Negre, N., Li, T.R., Cavalli, G., Zhao, H., Van Steensel, B., and White, K.P. (2003). Protein-DNA interaction mapping using genomic tiling path microarrays in Drosophila. Proceedings of the National Academy of Sciences of the United States of America *100*, 9428-9433.

Tanimoto, H., Itoh, S., ten Dijke, P., and Tabata, T. (2000). Hedgehog creates a gradient of DPP activity in Drosophila wing imaginal discs. Molecular cell *5*, 59-71.

Tolhuis, B., de Wit, E., Muijrers, I., Teunissen, H., Talhout, W., van Steensel, B., and van Lohuizen, M. (2006). Genome-wide profiling of PRC1 and PRC2 Polycomb chromatin binding in Drosophila melanogaster. Nature genetics *38*, 694-699.

van Steensel, B., Delrow, J., and Bussemaker, H.J. (2003). Genomewide analysis of Drosophila GAGA factor target genes reveals context-dependent DNA binding. Proceedings of the National Academy of Sciences of the United States of America *100*, 2580-2585.

Xiang, Y., Yuan, Q., Vogt, N., Looger, L.L., Jan, L.Y., and Jan, Y.N. (2010). Light-avoidance-mediating photoreceptors tile the Drosophila larval body wall. Nature *468*, 921-926.